

## Supplementary Materials for

### **$^{238}\text{U}/^{235}\text{U}$ Measurement in Single-Zircon Crystals: Implications for the Hadean Environment, Magmatic Differentiation and Geochronology**

François L.H. Tissot\*, Mauricio Ibanez-Mejia, Patrick Boehnke, Nicolas Dauphas, David McGee, Timothy L. Grove, Mark T. Harrison.

\*Correspondence to: [tissot@caltech.edu](mailto:tissot@caltech.edu)

#### **This PDF file includes:**

Additional notes on Materials and Methods  
Supplementary Text  
Supplementary Figs. S1 to S11  
Supplementary Tables S1 to S5

#### **Additional notes on Materials and Methods**

##### S1. Reference zircons

Three reference zircon localities were measured: (i) FC-1, from an anorthosite in the Duluth Complex (Minnesota, USA),  $^{207}\text{Pb}/^{206}\text{Pb}$  age = 1098 Ma ([Paces and Miller, 1993](#); [Mattinson, 2010](#)), (ii) R33, from a monzodiorite in the Braintree Complex (Vermont, USA),  $^{207}\text{Pb}/^{206}\text{Pb}$  age = 420 Ma ([Black et al., 2004](#); [Mattinson, 2010](#)), and (iii) Temora, from a gabbroic diorite in the Lachlan Fold Belt (Australia),  $^{207}\text{Pb}/^{206}\text{Pb}$  age = 418 Ma ([Black et al., 2004](#); [Mattinson, 2010](#)).

##### S2. Sample picking

Reference zircons (FC-1, R33 and Temora) were generously provided by J. Ramezani (Bowring group, MIT) as annealed grains. Jack Hills zircons were obtained as grains in an epoxy mount previously used for SHRIMP U-Pb dating ([Holden et al., 2009](#)). Individual grains were picked from the mount under a binocular microscope using stainless steel tools. To prevent grains from flying out of the mount, a few drops of ethanol were added onto the mount. Extracted zircons were temporarily placed into clean quartz vials in MQ water. The glass vials were then brought into the Bowring class 100 clean laboratory (MIT) and transferred to clean 7 mL Teflon beakers.

##### S3. Extra details on data quality control tests for $\delta^{238}\text{U}$ values

###### S3.1. Geostandards

To assess the accuracy of the U isotope measurements, four replicates of the Columbia River basalt (BCR-2) were prepared, processed along and measured with the zircon samples. Fresh powder aliquots were digested by successive acid attack (at least 24 hr each) on hot plate in (1) 4 mL of HF-HNO<sub>3</sub> (3:1) at 160°C, (2) 4 mL of HCl-HNO<sub>3</sub> (3:1) at 140°C, (3) 4 mL of HF-HNO<sub>3</sub> (3:1) at 160°C, and (4) 4 mL of HCl-HNO<sub>3</sub> (3:1) at 140°C. After each HF step, ~ 50  $\mu\text{L}$  of HClO<sub>4</sub>

(perchloric acid) was added to the samples before complete dry down (to remove fluorides). After full digestion, the geostandards were taken back in 3 M HNO<sub>3</sub> + 0.02 M oxalic acid, processed along with the samples and measured several times during each measurement session. For each replicate, about 250 ng of U was analyzed, and the average  $\delta^{238}\text{U}$  obtained are both reproducible ( $-0.23 \pm 0.06 \text{ ‰}$ ,  $-0.27 \pm 0.05 \text{ ‰}$ ,  $-0.27 \pm 0.04 \text{ ‰}$  and  $-0.26 \pm 0.04 \text{ ‰}$ , Supplementary Table S5) and indistinguishable from the average value of  $-0.27 \pm 0.05 \text{ ‰}$  (95% CI), which includes data from 11 studies ([Tissot and Dauphas, 2015](#), supplementary material). Furthermore, the  $\delta^{238}\text{U}$  values measured during each session with a similar number of solution analysis as the one used for zircons (n between 1 and 8), are all within error of the average value (Fig. 2a), demonstrating the reliability of the accuracy and precision of our measurements.

### S3.2. Variable matrices

To test if the sample matrix influenced the measurements, two carbonate geostandards, the crinoïdic limestone CCH-1 and the dolomite DWA-1, were also analyzed. These samples were prepared in the same way as the BCR-2 samples. As for BCR-2,  $\delta^{238}\text{U}$  values measured in each session are highly reproducible and all within error of each other (Supplementary Table S5).

### S3.3 Zr doping tests

To ensure that the residual amount of Zr present in the purified U fraction would not affect the U isotopic analysis, a doping test was performed. Aliquots were taken from a spiked solution of the CRM-112a U standard, with a  $U_{\text{Sp}}/U_{\text{Smp}}$  of 3 %, and were doped with Zr to achieve Zr/U atomic ratios ranging from 0.05 to 10. These solutions were measured on the Neptune MC-ICPMS (U. of Chicago) using the same setup used for sample measurements (*i.e.*, 14 V on  $^{238}\text{U}$ , 50 cycles of 4.194 second of integrations time). Every Zr-doped solutions analysis was bracketed by measurements of a 3 % spiked CRM-112a solution (not doped with Zr). The  $\delta^{238}\text{U}$  obtained on the Zr-doped solutions are indistinguishable from 0 ‰ (relative to the CRM-112a standard, Fig. 2b), indicating that the presence of Zr at the levels tested does not affect the U isotope measurements. Because Zr is notorious for sticking to the walls of the nebulizer and other inlet tubings, a BCR-2 solution was measured every two Zr-doped solutions to test for potential matrix effect associated with delayed release of Zr. These four BCR-2 solution analyses gave  $\delta^{238}\text{U}$  values of  $-0.24 \pm 0.13 \text{ ‰}$ ,  $-0.24 \pm 0.13 \text{ ‰}$ ,  $-0.23 \pm 0.13 \text{ ‰}$  and  $-0.35 \pm 0.13 \text{ ‰}$ , indistinguishable from the expected value of  $-0.27 \pm 0.05 \text{ ‰}$  (95% CI, [Tissot and Dauphas, 2015](#)).

### S4. Data quality control for $\delta(^{234}\text{U})$ values

The  $(^{234}\text{U}/^{238}\text{U})$  activity ratios relative to secular equilibrium are reported as:  $\delta(^{234}\text{U}) = [(^{234}\text{U}/^{238}\text{U})_{\text{sample}} / (^{234}\text{U}/^{238}\text{U})_{\text{eq}} - 1] \times 10^3$ , where  $(^{234}\text{U}/^{238}\text{U})_{\text{eq}}$  is the atomic ratio at secular equilibrium:  $\lambda_{238}/\lambda_{234} = (1.5513 \times 10^{-10}) / (2.8220 \times 10^{-6}) = 5.4969 \times 10^{-5}$  ([Cheng et al., 2013](#)). The same quality tests discussed above for  $\delta^{238}\text{U}$  values can be applied to the  $\delta(^{234}\text{U})$  values.

1) The average  $\delta(^{234}\text{U})$  values obtained on replicate aliquots of the BCR-2 geostandards are both reproducible ( $+0.2 \pm 2.2 \text{ ‰}$ ,  $+2.9 \pm 2.1 \text{ ‰}$ ,  $0.0 \pm 0.2 \text{ ‰}$  and  $+0.8 \pm 0.2 \text{ ‰}$ ) and indistinguishable from the average value of  $+0.3 \pm 1.6 \text{ ‰}$  (95% CI), which includes data from 3 studies ([Tissot and Dauphas, 2015](#), supplementary material). The difference in uncertainties is due to difference in the measurement setup (Table 2) with large uncertainties corresponding to  $^{234}\text{U}$  measurement on faraday cup and small uncertainties to  $^{234}\text{U}$  measurement on the SEM. The  $\delta(^{234}\text{U})$  values measured

during each session are all within error of the average value. The small but resolvable difference between the average results of BCR-2 replicate c ( $0.0 \pm 0.2 \text{ ‰}$ ) and d ( $+0.8 \pm 0.2 \text{ ‰}$ ) could be due to minor heterogeneity of the geostandards powder, or a slight underestimation of the uncertainties on the  $\delta(^{234}\text{U})$  data. Such a small difference is negligible when compared to the magnitude of  $\delta(^{234}\text{U})$  variations in the samples (from  $-339.8$  to  $+185.0 \text{ ‰}$ , Supplementary Fig. S4 and Table S4) and therefore do not influence the conclusions of this study.

2) The  $\delta(^{234}\text{U})$  values obtained on the two carbonate standards (CCH-1 and DWA-1) measured to assess potential matrix effect were highly reproducible in all sessions (Supplementary Table S3).

3) The very good agreement between the SSB and DS data (Supplementary Fig. S2) further strengthens our confidence in the precision and accuracy of the measurements. Most samples have SSB and DS  $\delta(^{234}\text{U})$  values within uncertainty of each other (Supplementary Table S4) and for samples measured at high-precision (O.L. set up), the difference  $\delta(^{234}\text{U})_{\text{DS}} - \delta(^{234}\text{U})_{\text{SSB}}$  is on average  $-0.5 \text{ ‰}$ , and is always smaller than  $3.5 \text{ ‰}$ .

4) Finally, comparison of our  $\delta(^{234}\text{U})$  data with that of [Hiess et al. \(2012\)](#) (Supplementary Fig. S3 and Table S5) shows again the accuracy, and the greater precision, of our analyses. The minor difference observed for the R33 reference zircon ( $2.1 \pm 0.6 \text{ ‰}$  in this work, vs.  $-3.6 \pm 4.8 \text{ ‰}$  in [Hiess et al., 2012](#)) is likely due to the fact that single grains were used in the present work, while hundreds/thousands of grains were used by [Hiess et al. \(2012\)](#). Indeed, depending on the grain size and geometry, variable amounts of  $^{234}\text{U}$  will be lost by alpha-recoil, which would result in some variability in the  $\delta(^{234}\text{U})$  values measured from grain to grain.

Overall, the above tests show the reliability of the  $\delta(^{234}\text{U})$  data reported herein.

#### S5. Achieved vs. achievable precision

In this study, each sample measurement is bracketed by two standard measurements as follows: STD-SMP-STD. Standard and samples are measured in similar conditions (same spiking level, same concentration, same acid molarity), which means that similar internal uncertainties are associated with both types of analysis. To take into account the uncertainty associated with the standard measurement, the uncertainties reported on a sample measurement are “2SE external reproducibility” calculated as  $2 \times \sigma_{\text{Standard}} / \sqrt{n}$ , where  $2 \times \sigma_{\text{Standard}}$  is the daily external reproducibility of repeat measurements of the standard CRM-112a bracketed by itself, and  $n$  is the number of sample solution measurements. In most cases, this calculation yields the same result as quadratically adding the uncertainties on the sample and bracketing standard measurements, and, as these are similar in magnitude, is equivalent to multiplying by a factor  $\sqrt{2}$  the uncertainty on the sample measurement.

The precision (2SE external) achieved in this study is shown in Fig. S5 as a function of the amount of U measured and is compared to the lower limit theoretically achievable with the instrument setup used, calculated using (S.17) (below). These theoretical curves correspond to the quadratic sum of the counting statistics and Johnson noise uncertainties relevant to the measurement setup used:  $^{238}\text{U}/^{235}\text{U}$  ratios measured with a  $^{233}\text{U}$ - $^{236}\text{U}$  double spike on either Neptune MC-ICPMS or Nu-Plasma II-ES MC-ICPMS (see Table 2). Following the notation of [Dauphas et al. \(2014\)](#), counting statistic and Johnson noise uncertainties are calculated, respectively, as:

$$\sigma_{counting}^2 = n = Ut/(eR), \quad (S.3) \quad \text{and} \quad \sigma_j^2 = 4kTt/(e^2R), \quad (S.4)$$

where  $n$  is the total counts measured in the mass spectrometer for a given isotope,  $U$  is the corresponding voltage (in V) measured on the collector,  $e$  the element charge ( $1.602 \times 10^{-19}$  C),  $R$  is the amplifier resistance (in ohm),  $t$  is the total integration time (in seconds),  $k$  is Boltzmann's constant ( $1.381 \times 10^{-23}$  m<sup>2</sup> kg s<sup>-2</sup> K<sup>-1</sup>) and  $T$  is the temperature of the detector (in K), typically 46°C on the Neptune. To calculate the uncertainty corresponding to a total amount of U measured, the average amount of U consumed per cycle (4.194 seconds) of analysis on each instrument is taken into account (0.212 ng U / cycle for the Nu-II and 0.082 ng U / cycle for the Neptune). The relative uncertainty on ion counts for a given isotope  $i$  is noted (Eq. A.3 in [Dauphas et al., 2014](#)),

$$X_i = \frac{\sigma_i^2}{n_i^2} = \frac{\sigma_{counting}^2 + \sigma_j^2}{n_i^2} = \frac{n_i + \sigma_j^2}{n_i^2} = \frac{1}{n_i} + \frac{\sigma_j^2}{n_i^2}. \quad (S.5)$$

Considering 4 isotopes  $a, b, c, d$ , the relative error on the measured isotopic ratio  $r_{b/a} = n_b/n_a$  is therefore (Eq. A.5 in [Dauphas et al., 2014](#)),

$$\left(\frac{\sigma_{rb/a}}{r_{b/a}}\right)^2 = \frac{n_b + \sigma_{jb}^2}{n_b^2} + \frac{n_a + \sigma_{ja}^2}{n_a^2} = X_b + X_a. \quad (S.6)$$

For an isotopic ratio that has not been corrected for mass-fractionation, and noting  $A_i$  the abundance of isotope  $i$  in some reference material, the measured ratio  $r_{b/a}$  can be expressed in  $\delta'$  notation as (Eq. A.6 in [Dauphas et al., 2014](#)),

$$\delta'_{b/a} = 10^3 \ln\left(\frac{r_{b/a}}{A_b/A_a}\right) \simeq 10^3 \left(\frac{r_{b/a}}{A_b/A_a} - 1\right) \simeq \delta_{b/a}, \quad (S.7)$$

and its associated error is then (Eq. 59 in [Albarede et al., 2004](#) and Eq. A.7 [Dauphas et al., 2014](#))

$$\sigma_{\delta'_{b/a}}^2 = 10^6 (\sigma_{rb/a}/r_{b/a})^2 = 10^6 (X_b + X_a) \simeq \sigma_{\delta_{b/a}}^2. \quad (S.8)$$

Here, measurements are done using a U double-spike to correct for mass fractionation during sample preparation and isotopic analysis. Because the double-spike contains negligible amounts of <sup>238</sup>U and <sup>235</sup>U, and the spiked isotopes are not naturally occurring, the mass-bias correction using the spike can essentially be described as an internal normalization to a second ratio,  $R_{d/c}$ , using the exponential law as,

$$r_{d/c} = R_{d/c} (m_d/m_c)^\beta, \quad (S.9)$$

with  $m_i$  the mass of isotope  $i$ , and  $R_{d/c} = A_d/A_c$ . The fractionation factor beta, is thus equal to

$$\beta = \ln(r_{d/c}/[A_d/A_c]) / \ln(m_d/m_c). \quad (S.10)$$

The double-spike corrected ratio  $R_{b/a}^*$  (noted with a star superscript) is thus,

$$R_{b/a}^* = \frac{r_{b/a}}{(m_b/m_a)^\beta}. \quad (S.11)$$

To convert (S.11) in  $\delta'$  notation, we divide it by the standard isotopic ratio  $A_b/A_a$ , take the natural logarithm, and multiply by  $10^3$ , which gives,

$$\delta'_{b/a^*} = 10^3 \ln \left( \frac{r_{b/a}}{A_b/A_a} \right) - 10^3 \frac{\ln(m_b/m_a)}{\ln(m_d/m_c)} \ln \left( \frac{r_{d/c}}{A_d/A_c} \right). \quad (\text{S.12})$$

Noting  $\mu_{j/i} = \ln(m_j/m_i)$ , (S.12) becomes,

$$\delta'_{b/a^*} = 10^3 \left[ \ln \frac{n_b}{A_b} - \ln \frac{n_a}{A_a} + \frac{\mu_{b/a}}{\mu_{d/c}} \left( \ln \frac{n_c}{A_c} - \ln \frac{n_d}{A_d} \right) \right], \quad (\text{S.13})$$

In the special case where  $a=c$ , (S.13) simplifies into Eq. A.19 of [Dauphas et al. \(2014\)](#). The error on  $\delta'_{b/a^*}$  then takes the form,

$$\sigma_{\delta'_{b/a^*}}^2 = 10^6 \left[ X_b + X_a + \left( \frac{\mu_{b/a}}{\mu_{d/c}} \right)^2 (X_c + X_d) \right]. \quad (\text{S.14})$$

In the specific case at hand  $a$  is  $^{235}\text{U}$ ,  $b$  is  $^{238}\text{U}$ ,  $c$  is  $^{233}\text{U}$  and  $d$  is  $^{236}\text{U}$ . Because the double-spike has a  $^{233}\text{U}/^{236}\text{U}$  ratio close to unity ( $1.01906 \pm 0.00016$ , [Verbruggen et al., 2008](#)),  $^{233}\text{U}$  and  $^{236}\text{U}$  will typically be measured using the same type of amplifiers, and  $X_{233} \approx X_{236}$ . The error on  $\delta^{238}\text{U}$  values measured with the IRMM-3636 double spike will therefore be,

$$\sigma_{\delta^{238/235}'}^2 \approx 10^6 \left[ X_{238} + X_{235} + 2 \left( \frac{\mu_{8/5}}{\mu_{6/3}} \right)^2 X_{236} \right], \quad (\text{S.15})$$

$$\sigma_{\delta^{238/235}'}^2 \approx 10^6 \left[ \frac{1}{n_8} + \frac{\sigma_{j8}^2}{n_8^2} + \frac{1}{n_5} + \frac{\sigma_{j5}^2}{n_5^2} + 2 \left( \frac{\mu_{8/5}}{\mu_{6/3}} \right)^2 \left( \frac{1}{n_6} + \frac{\sigma_{j6}^2}{n_6^2} \right) \right]. \quad (\text{S.16})$$

The number of atoms of  $^{236}\text{U}$  measured will depend on the amount of spike added to the sample and can be expressed as  $n_6 = p n_8$ , where  $p = U_{\text{Spike}}/U_{\text{Sample}} \times Ab_{\text{Sp}}^{236}/Ab_{\text{Smp}}^{238}$  and  $Ab^i$  refers to the abundance of isotope  $i$  in the spike “sp” or sample “smp”. Assuming that variations in the  $^{238}\text{U}/^{235}\text{U}$  ratio are small, we can write that  $n_5 = n_8/R_U$ , where  $R_U$  is the average crustal  $^{238}\text{U}/^{235}\text{U}$  ratio of 137.797 ([Tissot and Dauphas, 2015](#)). Equation (S.16) takes the final form,

$$\sigma_{\delta^{238/235}'}^2 \approx 10^6 \left\{ \frac{1}{n_8} \left[ 1 + R_U + \frac{2 \left( \frac{\mu_{8/5}}{\mu_{6/3}} \right)^2}{p} \right] + \frac{1}{n_8^2} \left[ \sigma_{j8}^2 + \sigma_{j5}^2 R_U^2 + 2 \frac{\sigma_{j6}^2 \left( \frac{\mu_{8/5}}{\mu_{6/3}} \right)^2}{p^2} \right] \right\}. \quad (\text{S.17})$$

The first term on the right-hand side of Eq. (S.17) describes counting statistics uncertainties, while the second term describes Johnson Noise uncertainties. The above equation yields an uncertainty estimate for an individual measurement, not taking into account sample-standard bracketing. To do so, and obtain a “2 SE external reproducibility” estimate, we multiply the results from (S.17) by a factor  $\sqrt{2}$  (see above).

In this work, the  $^{238}\text{U}$  signal intensity varied between 10 and 20 V depending on the sample, so two curves are shown for each instrumental setup on Fig. S5. We find that the external reproducibility of the measurements in this study is in excellent agreement with the theoretical lower limits calculated using (S.17), which further testifies to the high quality of our data. The

significantly higher uncertainties obtained on the Nu-Plasma II (MIT) appear to be mainly explained by the lower sensitivity of this instrument compared to the Neptune (U. of Chicago) (Supplementary Fig. S5, compare grey curves on panel a and b). Yet, some analyses conducted on the Nu-II show slightly higher uncertainties than predicted by (S.17), which indicates that some other factors, likely to be linked to instabilities in the plasma and/or sample introduction (*i.e.*, desolvating nebulizer), affected these measurements.

## Supplementary Text

### S6. Age corrections

A difference between the actual and assumed sample  $^{238}\text{U}/^{235}\text{U}$  used to calculate a sample's age (such as the traditional “consensus” value of 137.88 from [Steiger and Jager, 1977](#), or the newly recommended value of 137.818 from [Hiess et al., 2012](#)) will result in inaccurate ages.

The  $^{207}\text{Pb}$ - $^{206}\text{Pb}$  age corrections (or offsets,  $\Delta t$ ) will depend on the uncorrected age of the sample ( $t$ ), and the difference between the actual and assumed U isotope composition of the sample (noted  $\Delta U = (^{238}\text{U}/^{235}\text{U}_{\text{Actual}}/^{238}\text{U}/^{235}\text{U}_{\text{Assumed}} - 1) \cdot 1000$ ), as (Eq. 12 in [Tissot and Dauphas, 2015](#)):

$$\Delta t = \frac{\Delta U \cdot (e^{\lambda_{238} \cdot t} - 1) \cdot (e^{\lambda_{235} \cdot t} - 1)}{1000 \cdot (\lambda_{238} \cdot e^{\lambda_{238} \cdot t} - \lambda_{235} \cdot e^{\lambda_{235} \cdot t} + (\lambda_{235} - \lambda_{238}) \cdot e^{(\lambda_{235} + \lambda_{238}) \cdot t})}. \quad (\text{S.18})$$

Though theoretically independent of variations in the  $^{238}\text{U}/^{235}\text{U}$  ratio of the sample, U-Pb ages are, in practice, also impacted and age corrections will depend on the same  $t$  and  $\Delta U$  values as well as parameters specific to the spike used for the U-Pb measurement. Taking the example of the popular EARTHTIME distributed ‘ET535 tracer’ (a mixed  $^{205}\text{Pb}$ - $^{233}\text{U}$ - $^{235}\text{U}$  tracer), the assumption of knowledge of the sample  $^{238}\text{U}/^{235}\text{U}$  ratio (noted  $R_U$ ) directly impacts two parameters that affect Pb-Pb and U-Pb ages:

(1) the amount of  $^{235}\text{U}$  in the sample, which is calculated as:

$$^{235}\text{U}_s = \frac{1}{R_U} \cdot ^{238}\text{U}_s \quad (\text{S.19})$$

where s stands for “sample”.

(2) the degree of U isotopic fractionation, both instrumental and introduced during chemical separation, expressed as the “linear uranium fractionation factor”,  $F_U$ , defined as (Eq. 38 in [Schmitz and Schoene, 2007](#), with addition of the  $^{238}\text{U}$  blank term):

$$F_U = \frac{R_{35t} \cdot (R_U - R_{85m}) + R_{35m} \cdot (R_{85t} - R_U + ^{238}\text{U}b/^{235}\text{U}t)}{2 \cdot R_{35m} \cdot (R_{85t} - R_U + ^{238}\text{U}b/^{235}\text{U}t) + 3 \cdot R_{35t} \cdot R_{85m}}, \quad (\text{S.20})$$

where  $R_{ij}$  is the ratio of uranium isotope  $^i\text{U}/^j\text{U}$ , s, t and b stand for “sample”, “tracer” and “blank”, respectively, and m refers to “measured” ratios.

Since the fractionation factor  $F_U$  (i) depends on the assumed  $^{238}\text{U}/^{235}\text{U}$  ratio ( $R_U$ ), and (ii) is being used to correct all measured U isotopic ratios, the amount of  $^{238}\text{U}$  in the sample is going to depend on the assumed  $^{238}\text{U}/^{235}\text{U}$  ratio, as (Eq. 48 in [Schmitz and Schoene, 2007](#)):

$${}^{238}\text{U}_S = \frac{{}^{235}\text{U}t \cdot R_{85m} \cdot (1 + 3 \cdot FU) - (R_{85t} \cdot {}^{235}\text{U}t) - {}^{238}\text{U}b}{1 - \frac{1}{R_U} \cdot R_{85m} \cdot (1 + 3 \cdot FU)} \quad (\text{S.21})$$

For  ${}^{206}\text{Pb}$ - ${}^{238}\text{U}$  ages, the age equation is:

$$\frac{{}^{206}\text{Pb}^*}{{}^{238}\text{U}_S} = \left( e^{\lambda_{238} \cdot t\delta} - 1 \right) \quad (\text{S.22})$$

where the star denotes the radiogenic component, and  $t\delta$  is the time since closure of the system as calculated with the  ${}^{206}\text{Pb}$ - ${}^{238}\text{U}$  systematic. Because the variations on  $R_U$  (the  ${}^{238}\text{U}/{}^{235}\text{U}$  ratio) are small, the age correction will be small compared to the age of the sample, and we can write:

$$\Delta t\delta = \frac{\Delta R_U}{\partial R_U(t\delta)/\partial t\delta} \quad (\text{S.23})$$

By substituting (S.20) and (S.21) into (S.22), we get the expression of  $R_U(t\delta)$ , which is derived to obtain the following (Eq. S8 in [Tissot and Dauphas, 2015](#)):

$$\Delta t\delta = \frac{(1 - e^{-\lambda_{238} \cdot t\delta}) \cdot R_{85m}}{400 \cdot R_U - 1000 \cdot R_{85m}} \cdot \frac{\Delta U}{\lambda_{238}} \quad (\text{S.24})$$

where  $\Delta U$  is the difference between the actual and assumed U isotopic composition of the sample (in delta notation, ‰),  $t\delta$  is the  ${}^{206}\text{Pb}$ - ${}^{238}\text{U}$  age of the sample obtained using an “assumed” U isotopic composition, and  $\Delta t\delta$  is the age correction to apply to the sample age.

Similarly, for  ${}^{207}\text{Pb}$ - ${}^{235}\text{U}$  ages, the age equation is:

$$\frac{{}^{207}\text{Pb}^*}{{}^{235}\text{U}_S} = \left( e^{\lambda_{235} \cdot t5} - 1 \right) \quad (\text{S.25})$$

where the star denotes the radiogenic component, and  $t5$  is the time since closure of the system as calculated with the  ${}^{207}\text{Pb}$ - ${}^{235}\text{U}$  systematic. Here again, the age correction will be small compared to the age of the sample, and we can write:

$$\Delta t5 = \frac{\Delta R_U}{\partial R_U(t5)/\partial t5} \quad (\text{S.26})$$

By substituting (S.19), (S.20) and (S.21) into (S.25), we get the expression of  $R_U(t5)$ , which is derived to obtain the following:

$$\Delta t5 = \frac{(1 - e^{-\lambda_{235} \cdot t5})}{1000 - \frac{2500 \cdot R_{85m}}{R_U}} \cdot \frac{\Delta U}{\lambda_{235}} \quad (\text{S.27})$$

Note that this equation is slightly different from Eq S.14 in [Tissot and Dauphas \(2015\)](#), which was improperly derived and contained an extra term that increased age correction by ~2-4 %.

Together, (S.18), (S.24), (S.27) allow one to calculate the age corrections (or offsets) to apply to, respectively,  ${}^{207}\text{Pb}$ - ${}^{206}\text{Pb}$ ,  ${}^{206}\text{Pb}$ - ${}^{238}\text{U}$  and  ${}^{207}\text{Pb}$ - ${}^{235}\text{U}$  ages, as a function of the uncorrected age of

the sample ( $t$ ), the difference between the actual and assumed U isotope composition of the sample ( $\Delta U$ ), the value of the assumed  $^{238}\text{U}/^{235}\text{U}$  ratio ( $R_U$ ) and the EARTHTIME spike level ( $R85m = ^{238}\text{U}/^{235}\text{U}$  measured,  $\sim$  equivalent to the sample/tracer ratio, and typically equal to 1).

### S7. Impact on age concordance

Variability in the  $^{238}\text{U}/^{235}\text{U}$  ratio of a sample will also affect the concordance of the  $^{206}\text{Pb}$ - $^{238}\text{U}$  and  $^{207}\text{Pb}$ - $^{235}\text{U}$  ages. For a given value of  $\Delta U$  (difference between the actual and assumed U isotope composition of the sample), the  $^{206}\text{Pb}$ - $^{238}\text{U}$  age offset is much smaller than the  $^{207}\text{Pb}$ - $^{235}\text{U}$  age offset (55 times smaller for a 1 yr old sample, and 17 times smaller for a 4.55 Gyr old sample). In first approximation, it is therefore appropriate to assume that variations in the U isotope composition ( $R_U = ^{238}\text{U}/^{235}\text{U}$ ) will leave the ratio of radiogenic  $^{206}\text{Pb}$  to  $^{238}\text{U}$ , noted  $R68 = ^{206}\text{Pb}^*/^{238}\text{U}$ , unchanged and only impact the ratio of radiogenic  $^{207}\text{Pb}$  to  $^{235}\text{U}$ , noted  $R75 = ^{207}\text{Pb}^*/^{235}\text{U}$ . That is to say that in a  $^{206}\text{Pb}/^{238}\text{U}$  vs.  $^{207}\text{Pb}/^{235}\text{U}$  concordia diagram, variations in U isotope composition will move data points horizontally. The change in  $^{207}\text{Pb}^*/^{235}\text{U}$  ratio, noted  $\Delta R75$ , can simply be expressed as:

$$\Delta R75 = \frac{^{207}\text{Pb}^*}{^{206}\text{Pb}^*} \cdot \frac{^{206}\text{Pb}^*}{^{238}\text{U}} \cdot \Delta R_U, \quad (\text{S.28})$$

where  $\Delta R_U$  is the change in U isotope composition ( $^{238}\text{U}/^{235}\text{U}_{\text{Actual}} - ^{238}\text{U}/^{235}\text{U}_{\text{Assumed}}$ ). Replacing the

$^{207}\text{Pb}^*/^{206}\text{Pb}^*$  ratio by the transcendental age equation,  $\frac{^{207}\text{Pb}^*}{^{206}\text{Pb}^*} = \frac{1}{R_U} \cdot \frac{(e^{\lambda_{235} \cdot t} - 1)}{(e^{\lambda_{238} \cdot t} - 1)}$ , and expressing

$\Delta R_U$  as  $R_U \left( \frac{\Delta U}{1000} + 1 \right)$ , we obtain:

$$\Delta R75 = \frac{^{206}\text{Pb}^*}{^{238}\text{U}} \cdot \frac{(e^{\lambda_{235} \cdot t} - 1)}{(e^{\lambda_{238} \cdot t} - 1)} \cdot \left( \frac{\Delta U}{1000} + 1 \right). \quad (\text{S.29})$$

Using the same mathematical framework as in section S13, the assumption that U isotope variations do not impact the  $^{206}\text{Pb}^*/^{238}\text{U}$  ratio can be dropped, and analytical formulas quantifying the shifts in the  $^{206}\text{Pb}^*/^{238}\text{U}$  and  $^{207}\text{Pb}^*/^{235}\text{U}$  ratios, respectively noted  $\Delta R68$  and  $\Delta R75$ , can be derived. Because the variations in  $R_U$  (the  $^{238}\text{U}/^{235}\text{U}$  ratio) are small, the shift in concordia space will be small too, and we can write:

$$\Delta R68 = \frac{\Delta R_U}{\partial R_U(R68)/\partial R68}, \quad (\text{S.30}) \quad \text{and} \quad \Delta R75 = \frac{\Delta R_U}{\partial R_U(R75)/\partial R75}. \quad (\text{S.31})$$

By substituting (S.20) and (S.21) into  $R68 (= ^{206}\text{Pb}^*/^{238}\text{U})$ , we obtain the expression of  $R_U(R68)$ , which is derived to obtain the following:

$$\Delta R68 = \frac{(e^{\lambda_{238} \cdot t8} - 1) \cdot R85m}{400 \cdot R_U - 1000 \cdot R85m} \cdot \Delta U. \quad (\text{S.32})$$

Similarly, substituting (S.19), (S.20) and (S.21) into  $R75 (= ^{207}\text{Pb}^*/^{235}\text{U})$ , we obtain the expression of  $R_U(R75)$ , which is derived to obtain the following:

$$\Delta R75 = \frac{(e^{\lambda_{235} \cdot t5} - 1)}{1000 - \frac{2500 \cdot R85m}{R_U}} \cdot \Delta U \quad (\text{S.33})$$

For a given shift in U isotope composition, the equations governing the resulting shifts in concordia space are related to the ones governing the corresponding U-Pb age offsets, by:

$$\Delta R68 = \lambda_{238} \cdot e^{\lambda_{238} \cdot t} \cdot \Delta t8, \quad (\text{S.34}) \quad \text{and} \quad \Delta R75 = \lambda_{235} \cdot e^{\lambda_{235} \cdot t} \cdot \Delta t5, \quad (\text{S.35})$$

as expected given the functional forms of the age equations (S.22) and (S.25).

From (S.32), one can see that the shift in the  $^{206}\text{Pb}^*/^{238}\text{U}$  ratio is negligible in most cases (*i.e.*, when the shift in U isotope composition,  $\Delta U$ , is small). For instance, for a  $\sim 1$  Gyr old sample, a 3 ‰ shift in  $^{238}\text{U}/^{235}\text{U}$  ratio, will only result in a 0.1 ‰ shift in  $^{206}\text{Pb}^*/^{238}\text{U}$  ratio. On the other hand, the magnitude of the  $^{207}\text{Pb}^*/^{235}\text{U}$  ratio shift scales about 1:1 with the shift in  $^{238}\text{U}/^{235}\text{U}$  ratio, confirming the near horizontal displacement of data points in the concordia space stemming from U isotope variations.

### S8. Monte-Carlo simulations

To achieve higher precision and provide stronger temporal constraints, geochronological studies typically report the weighted mean age of  $\sim 15$ -20 zircon grains coming from the same rock. The assumption being that grains of similar apparent ages formed at the same time in the rock and thus belong to the same population. Because the U isotope composition of all grains is assumed to be the same and is not actually measured, the dispersion of the ages in the  $\sim 15$ -20 grains could theoretically be different (greater or smaller) than thought and the assumption of a single grain population might be invalid.

To quantify the effect of measuring the U isotope composition of single zircon grains on the weighted mean age of 20 zircon grains, we conducted a series of Monte-Carlo simulations. Assuming a typical EARTHIME spike run where the measured  $^{238}\text{U}/^{235}\text{U}$  ratio is equal to 1, only three parameters influence the dispersion of ages within a 20 grain population: (i) the offset between the actual and assumed U isotope composition used to calculate the age, (ii) the age of the sample, which impacts the age offset corresponding to a given difference between assumed and actual U isotope composition, and (iii) the precision of the age measurement of each individual grain. We varied these three parameters as follows:

- (1) Assuming a uniform distribution of  $\delta^{238}\text{U}$  values, centered on the values recommended by [Hiess et al. \(2012\)](#), and of width 1 ‰, a large number (here 50,000) of sets of 20 U isotope composition were randomly generated. Note that very similar results are obtained if a normal distribution of similar variance is used instead of the uniform distribution (the correspondence between uniform distribution width and normal distribution 2SD is  $2SD = 2\sqrt{\text{width}^2/12}$ , here 0.58 ‰, see Fig. 1). We present the results using the uniform distribution assumption, as it is more conservative: *i.e.*, for a given variance of  $\delta^{238}\text{U}$  the impact on the MSWD is slightly less important using the uniform distribution assumption.
- (2) For a given age (*e.g.*, 1000 Myr) and a given relative measurement precision (*e.g.*, 0.1 ‰), a series of 20 ages was created such that the MSWD of the weighted mean age of the initial

population was equal to 1 (Supplementary Fig. S8a). For instance, for a grain population of average age 1000 Myr, with errors on individual grain ages of 0.1 % (or 1 Myr) the age difference between each grain is  $\sim 0.084$  Myr, resulting in a weighted average age of 1000 Myr and a weighted error on the age of 0.223 Myr.

- (3) For each of the 20 grains, the  $^{207}\text{Pb}/^{206}\text{Pb}$ ,  $^{206}\text{Pb}/^{238}\text{U}$  and  $^{207}\text{Pb}/^{235}\text{U}$  age offsets resulting from the difference between the assumed U isotope composition (taken as the Hiess et al. ‘recommended value’) and the actual U isotope composition (randomly picked within the uniform distribution centered on the same ‘recommended value’) were calculated using analytical equations (S.18), (S.24), (S.27), leading to a U-corrected age distribution in the 20 grains. For simplicity, and to be conservative, the uncertainties on the age of each grain is kept constant before and after age correction, which means that only the improvement in accuracy is evaluated, and that the improvement in precision that can be brought by the U isotope measurement is not included in this calculation (see Fig. 8).
- (4) The MSWD of the U-corrected age distribution of the 20 grains was calculated for each of the 50,000 randomly generated sets of  $\delta^{238}\text{U}$  values, and the probability distribution function of these updated MSWD (Supplementary Fig. S6b) was then calculated.
- (5) Keeping the same 50,000 randomly generated set of 20  $\delta^{238}\text{U}$  values, steps 2-4 were repeated for 8 different relative age precisions (0.01, 0.02, 0.05, 0.1, 0.2, 0.5, 1 and 2 %) for 8 different sample ages (10, 100, 500, 1000, 2000, 3000, 4000, 4500 Myr) (Supplementary Fig. S6c and d).

The calculations were performed using the half-lives from [Jaffey et al. \(1971\)](#) ( $t_{1/2} = 0.70381$  Gyr for  $^{235}\text{U}$ , and  $t_{1/2} = 4.4683$  Gyr for  $^{238}\text{U}$ ), and the recommended  $^{238}\text{U}/^{235}\text{U}$  value from [Hiess et al. \(2012\)](#) ( $\delta^{238}\text{U} = -0.07981$  ‰ relative to CRM-112a, or 137.826 using the ratio of 137.837 for CRM-112a from [Richter et al., 2010](#)). The whole Monte-Carlo simulation (steps 1-5) was performed twice, assuming a uniform distribution of  $\delta^{238}\text{U}$  values over a 1 and 3 ‰ range, respectively.

The KDE (Kernel Density Estimation) for three different ages (10, 500, 3000 Ma) are shown in in Supplementary Fig. S7 ( $^{207}\text{Pb}/^{206}\text{Pb}$ ), Fig. S8 ( $^{206}\text{Pb}/^{238}\text{U}$ ) and Fig. S9 ( $^{207}\text{Pb}/^{235}\text{U}$ ). As the precision of the measurement increases, the MSWD of the U-corrected age distribution of 20 grains shifts away from unity, by up to several orders of magnitude, for both  $^{207}\text{Pb}/^{206}\text{Pb}$  ages and  $^{207}\text{Pb}/^{235}\text{U}$  ages. In the case of  $^{206}\text{Pb}/^{238}\text{U}$  ages, there is no significant shift away from unity for the U-corrected MSWD, and only a minor broadening of the KDE is observed as the precision of the measurement increases.

For all 8 age precisions and 8 ages investigated, the median shift in MSWD induced by U isotope measurement of single zircon grains is shown in Supplementary Fig. S10, while the width of the resulting MSWD KDEs are shown in Supplementary Fig. S11. For 20 grains (*i.e.*, 19 degrees of freedom), the low and high “critical” MSWD for a single grain population are 0.47 and 1.73, respectively ([Mahon, 1996](#)). Any shift in MSWD lower than 0.73 is therefore taken as not statistically significant, and a grey area denotes this region in Figs. S10 and S11. For a constant error in the  $^{207}\text{Pb}/^{206}\text{Pb}$  isotope measurement, the uncertainty on  $^{207}\text{Pb}/^{206}\text{Pb}$  ages increases as the sample ages decreases ([Amelin, 2006](#)). Therefore,  $^{207}\text{Pb}/^{206}\text{Pb}$  ages are hardly used for sample younger than 500-1000 Myr (grey vertical band in Fig. S10 and S11). Looking at Figs. S10 and

S11, it can easily be seen that measuring U isotope composition of single zircons becomes crucial for both  $^{207}\text{Pb}/^{206}\text{Pb}$  and  $^{207}\text{Pb}/^{235}\text{U}$  ages as soon as individual grain age precisions better than 0.05 to 0.10 % are achieved (MSWD shifting by more than 0.73 unit). This implies that at such high precision, and in the absence of U isotope measurements, rejecting grains based on their ages so as to achieve a unit MSWD (a common practice in geochronology) does not ensure that the grains selected to calculate a weighted mean age belong to a single age population. In fact, it is very likely that they do not, and measurement of U isotope on each zircon is required to properly assess whether grains belong to the same population and to calculate meaningful weighted mean ages.

Although the effect of single zircon U isotope measurements on  $^{206}\text{Pb}/^{238}\text{U}$  ages are inconsequential in the above in many cases (see above and Figs. S10 to S11), the existence of extreme outliers in the  $\delta^{238}\text{U}$  values of one pooled zircon (Table Cape, 19.9 Ma, which has  $^{238}\text{U}/^{235}\text{U}$  3.4 ‰ higher than the zircon recommended value, [Hiess et al., 2012](#)) means that even  $^{206}\text{Pb}/^{238}\text{U}$  ages might be affected in some rare occasions. For a 250 Myr old zircon, a difference of 3.4 ‰ between assumed and actual U isotope composition would translate into an age offset of  $\sim 15.4$  kyr. This is undoubtedly a small age offset, but similar in magnitude to the extent with which the end-Permian extinction is currently resolved from being an instantaneous event ( $60 \pm 48$  kyr, [Burgess et al., 2014](#)).

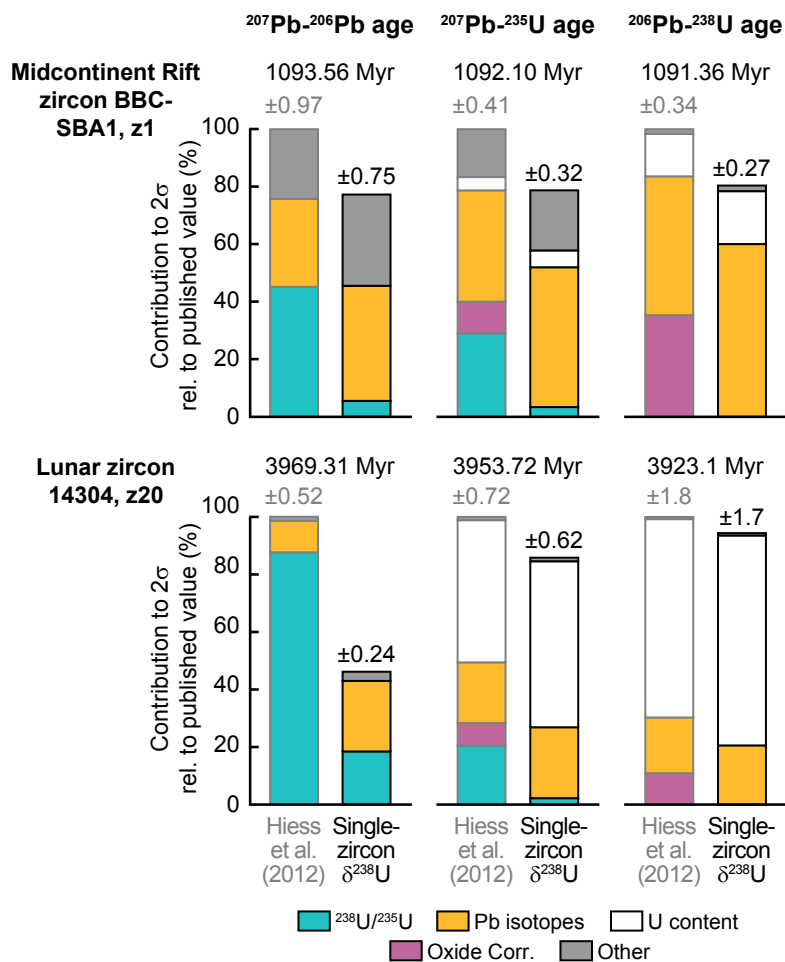


**Fig. S1.** Contribution of the different sources of uncertainty to high-precision Pb-Pb and U-Pb ages of a 1.09 Ga Midcontinent rift zircon (Fairchild et al., 2017) (top, sample BBC-SBA1, fraction z1) and a 3.97 Ga lunar zircon (Barboni et al., 2017) (bottom, sample 14304, fraction z20).  $^{206}\text{U}$ - $^{238}\text{Pb}$  and  $^{207}\text{Pb}$ - $^{206}\text{Pb}$  dates are typically reported for events younger and older, respectively, than  $\sim 1.5$  Ga. For each sample the published uncertainties calculated using the recommended  $^{238}\text{U}/^{235}\text{U}$  from Hiess et al. (2012) are compared to the uncertainties that would be achieved if a single-zircon U isotope measurement with uncertainty of  $\pm 0.10$  ‰ had been performed instead. Note that relative percentage uncertainties labeled “U content” coming from counting statistics on the amount of  $^{238}\text{U}$  in the sample would be much smaller using our method, given the higher sensitivity for U of MC-ICPMS instruments compared to TIMS.

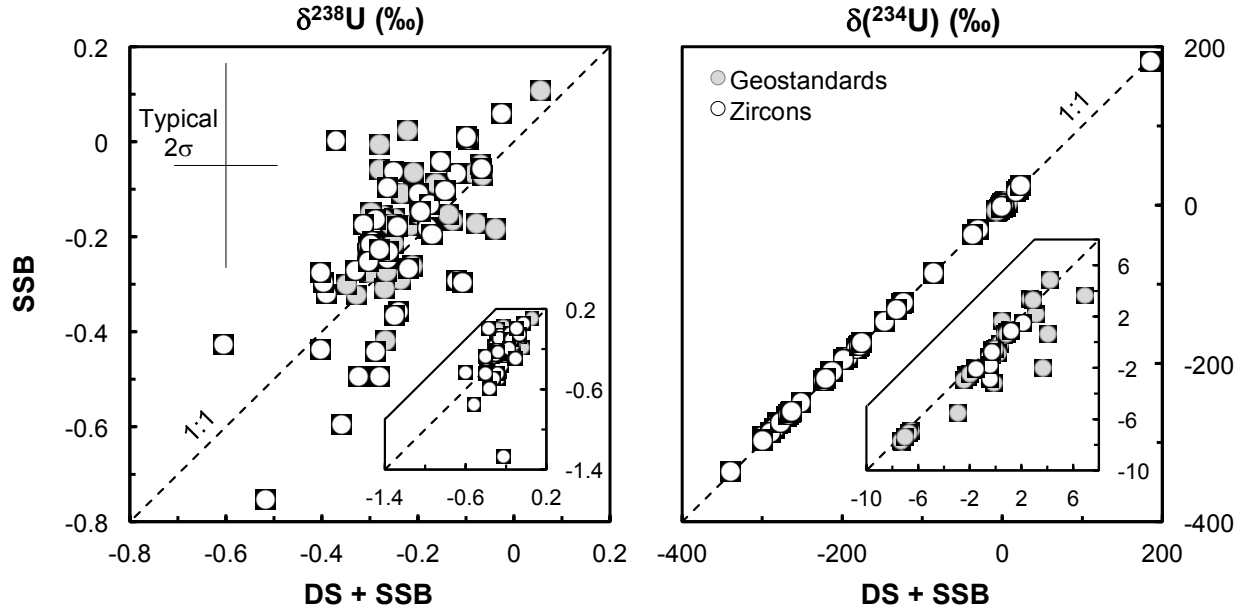


**Fig. S2.**  $\delta^{238}\text{U}$  (left) and  $\delta^{234}\text{U}$  (right) values obtained with the double-spike data reduction method (x-axis) plotted against the raw values measured, striped of the minor  $^{234}\text{U}$ ,  $^{235}\text{U}$  and  $^{238}\text{U}$  spike contribution (y-axis). All values are standard bracketed (SSB). The agreement of the two sets of values indicates that no resolvable matrix effects affected the measurements (for more details see [Tissot and Dauphas, 2015](#)).

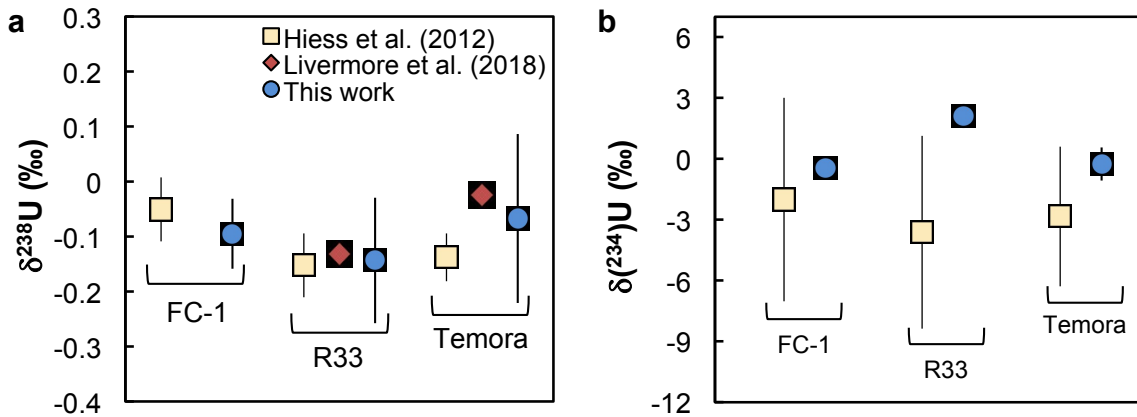


**Fig. S3.** Comparison of  $\delta^{238}\text{U}$  (top) and  $\delta^{234}\text{U}$  (bottom) values obtained in this study (circles), [Hiess et al. \(2012\)](#) (squares) and [Livermore et al. \(2018\)](#) (diamonds) on three reference zircons.

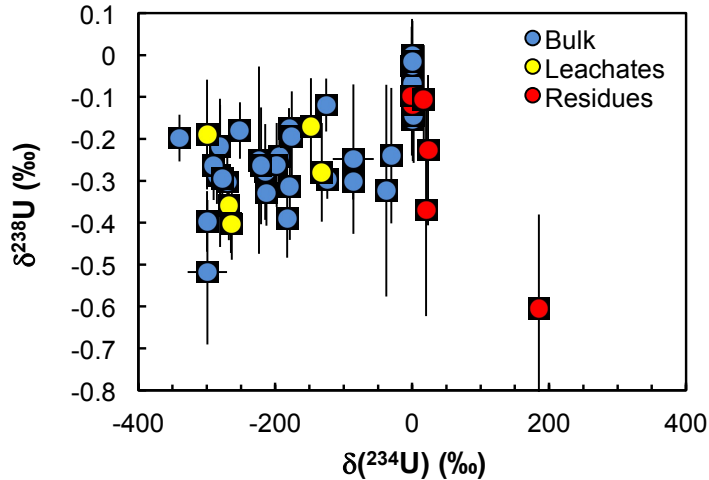


**Fig. S4.**  $\delta^{238}\text{U}$  vs.  $\delta^{234}\text{U}$  for zircon samples measured in this study. Large  $^{234}\text{U}$  depletions, most likely due to alpha-recoil loss of  $^{234}\text{U}$ , are found in both bulk zircons and chemically abraded zircon regions, while some bulk zircons and most zircon residues (after chemical abrasion) have  $\delta^{234}\text{U}$  values close to zero (*i.e.*, secular equilibrium).

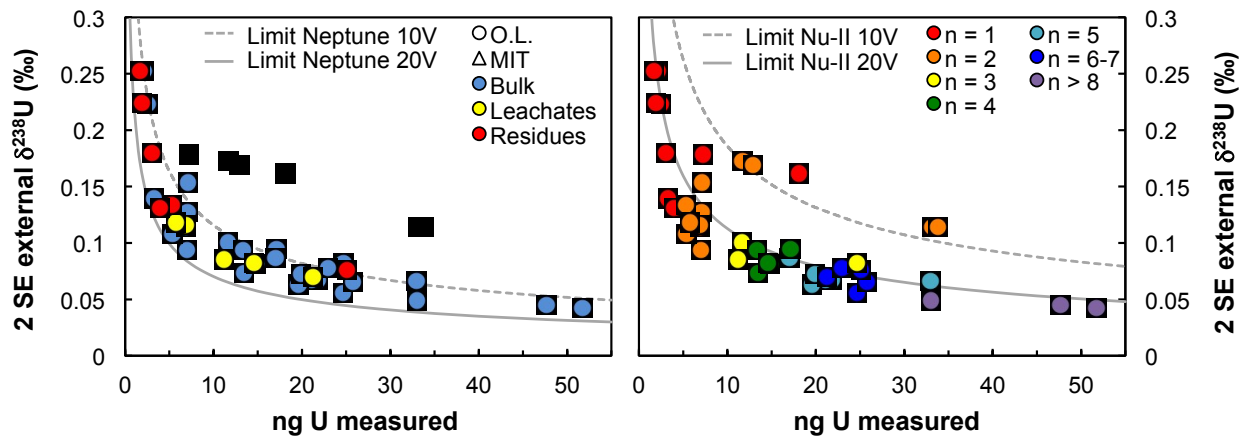


**Fig. S5.** Uncertainty on the  $\delta^{238}\text{U}$  values as a function of the amount of U measured (in ng). Uncertainties are shown as  $2 \times \sigma_{\text{Standard}}/\sqrt{n}$ , where  $2 \times \sigma_{\text{Standard}}$  is the daily external reproducibility of repeat measurements of the standard CRM-112a bracketed by itself, and  $n$  is the number of sample solution measurements. Grey curves show the theoretical lower limit achievable, calculated with equation (S.17), using either the Neptune MC-ICPMS (left panel) or the Nu-II ES MC-ICPMS (right panel) with  $^{238}\text{U}$  measured at 10 V (dotted grey curve) and 20 V (solid grey curve), and with both  $^{235}\text{U}$  and  $^{238}\text{U}$  measured using  $10^{11} \Omega$  resistors (see S10. *Achieved vs. achievable precision*). Note the different color-coding on the two panels. On the right panel,  $n$  is the number of solution analysis for each sample.

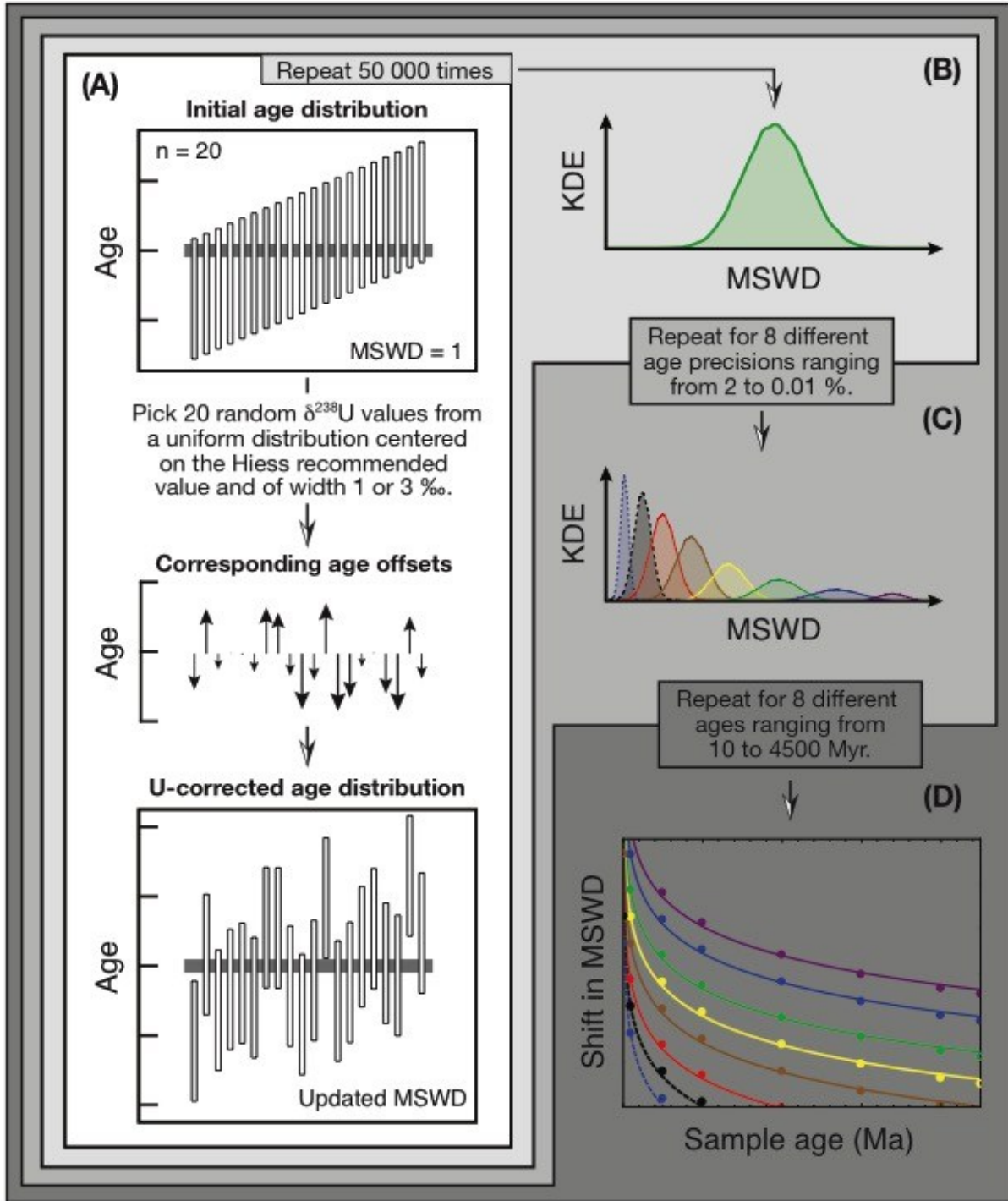


**Fig. S6.** Flow chart of the Monte-Carlo analysis performed to assess the effect of U isotope variability on the MSWD of weighted mean age of 20 grains. See S8. *Monte-Carlo simulations* for more details.

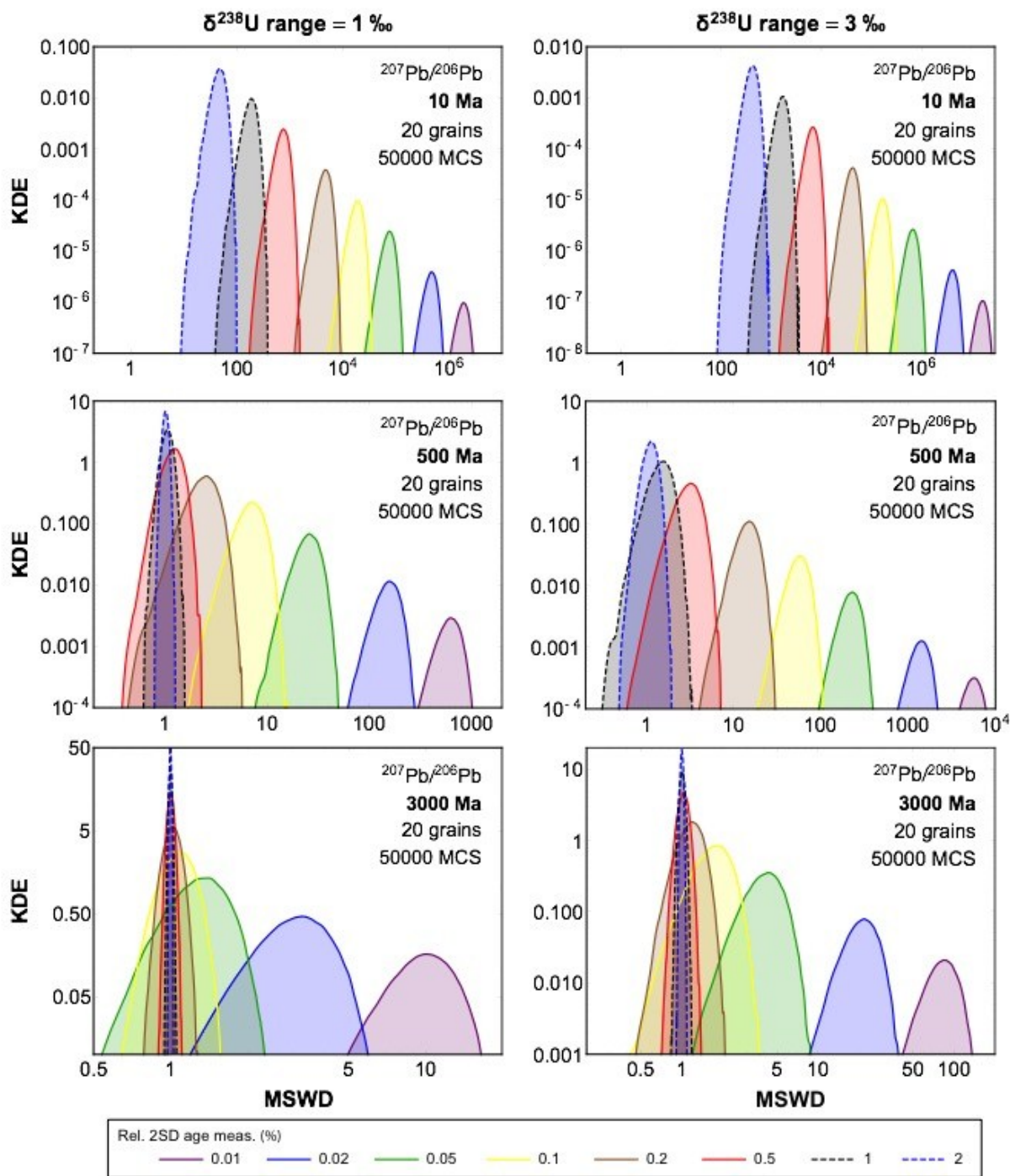


**Fig. S7.** KDE (Kernel Density Estimation) of the U-corrected MSWD of the  $^{207}\text{Pb}$ - $^{206}\text{Pb}$  weighted mean ages of 20 grains with U isotope composition randomly selected within a uniform distribution of width 1 ‰ (left) and 3 ‰ (right). Results shown for 3 sample ages, 10 Ma (top), 500 Ma (middle) and 3000 Ma (bottom). See *S8. Monte-Carlo simulations* for discussion.

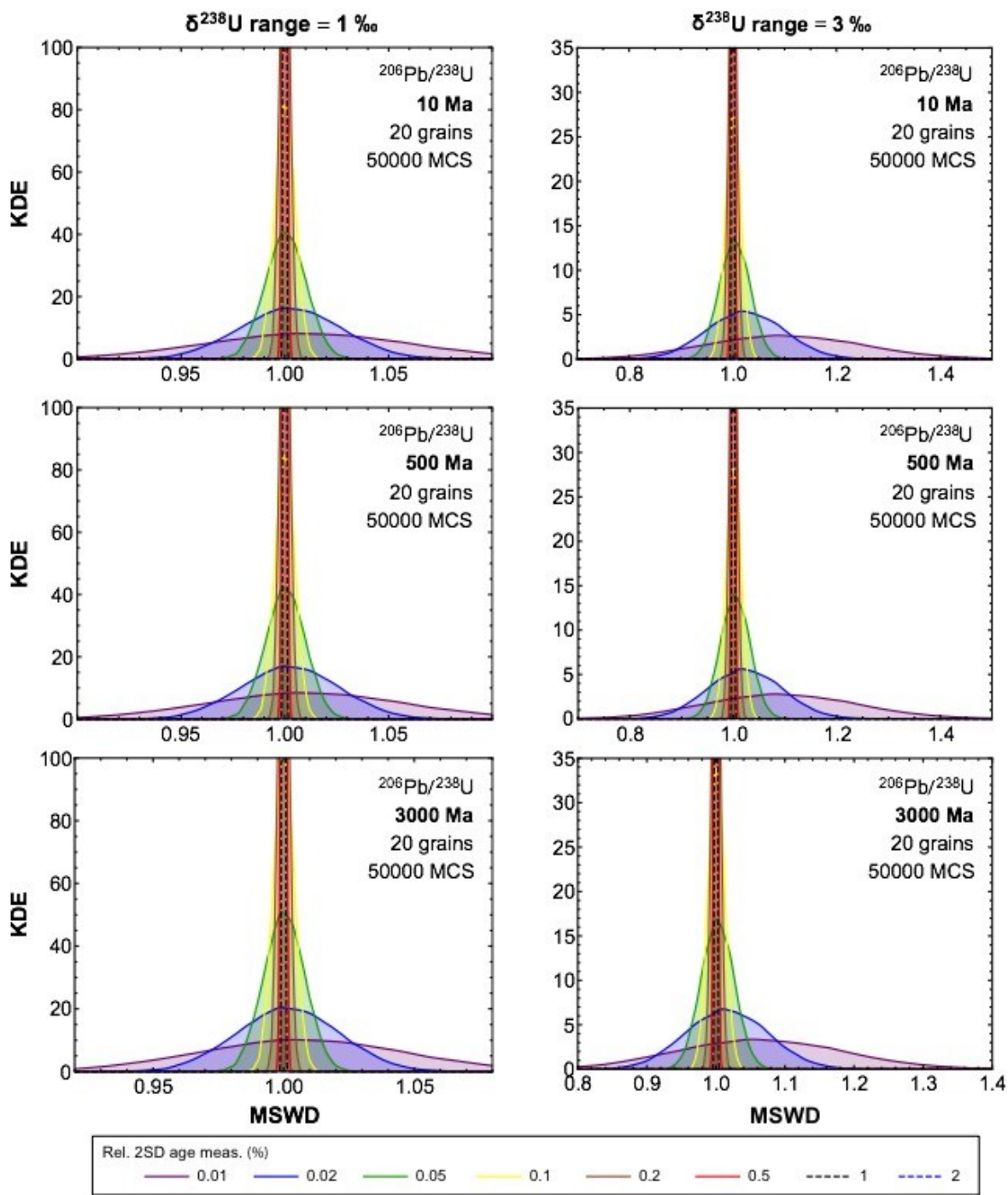


**Fig. S8.** Same as Fig. S7. but for  $^{206}\text{Pb}$ - $^{238}\text{U}$  weighted mean. See S8. Monte-Carlo simulations for discussion.

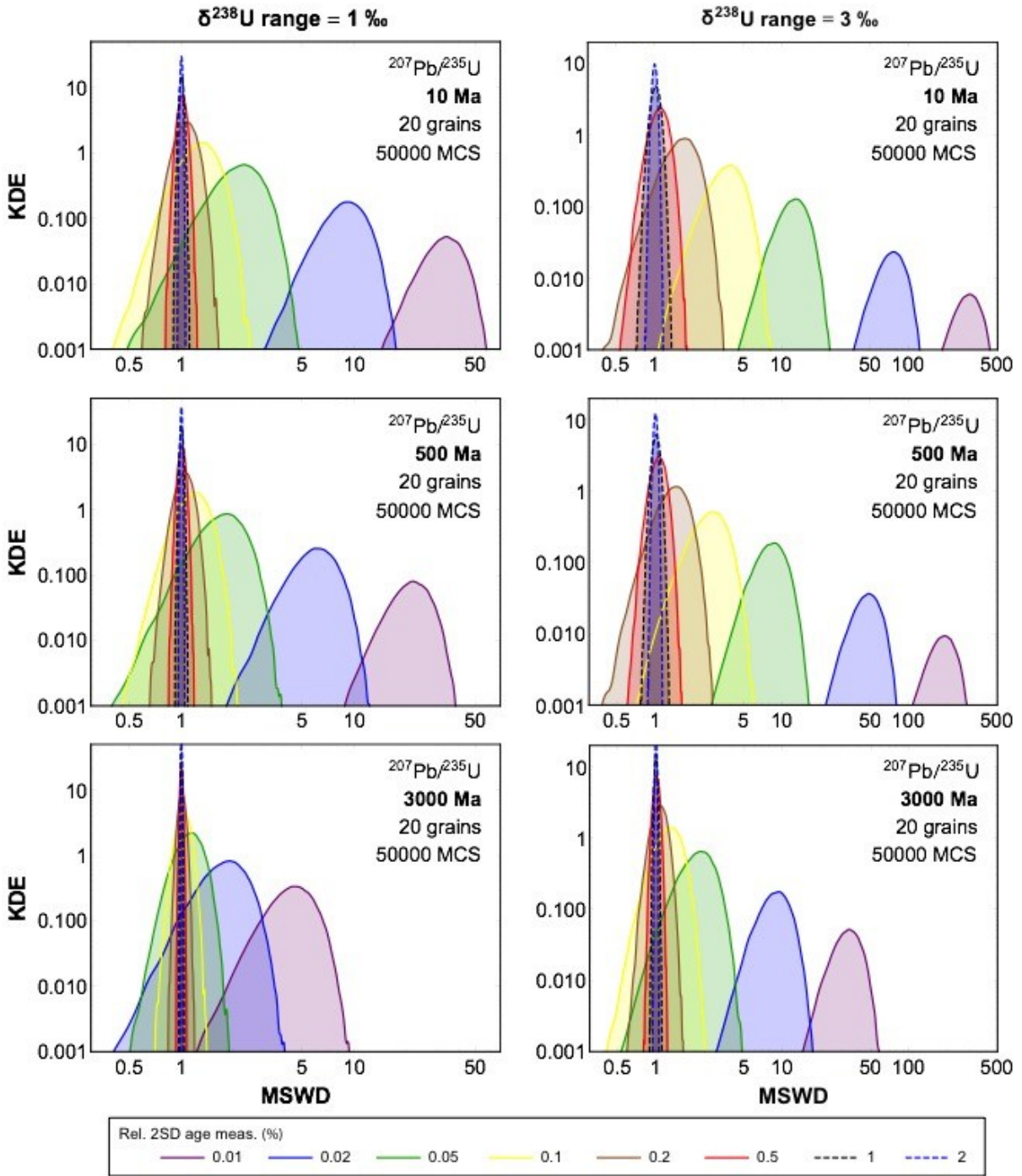


**Fig. S9.** Same as Fig. S7. but for  $^{207}\text{Pb}$ - $^{235}\text{U}$  weighted mean. See S8. Monte-Carlo simulations for discussion.

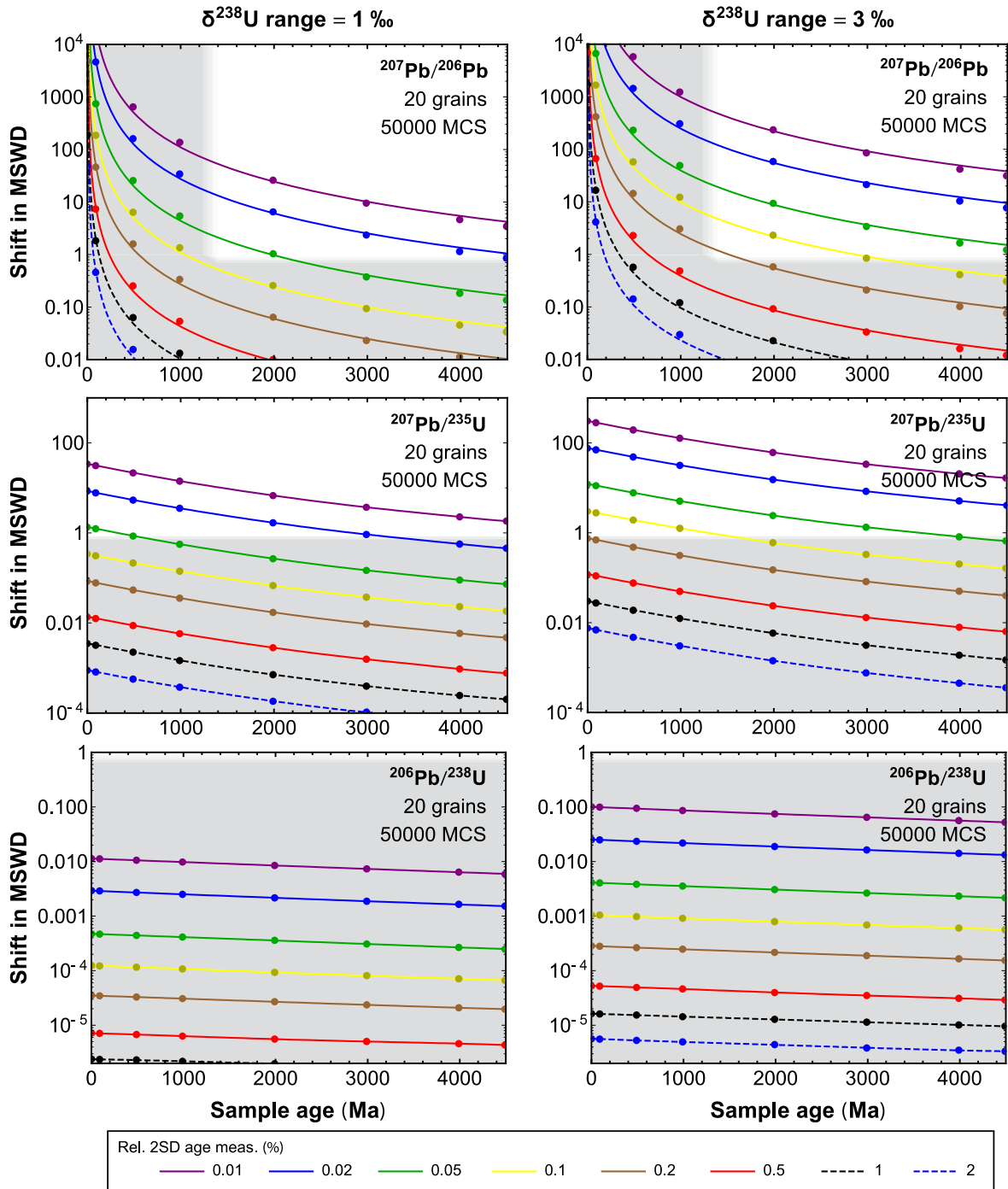


**Fig. S10.** Median shift in the MSWD of the weighted mean ages of 20 grains with U isotope composition randomly selected within a uniform distribution of width 1 ‰ (left) and 3 ‰ (right), as a function of age. Top, middle and bottom panels show results for, respectively,  $^{207}\text{Pb}$ - $^{206}\text{Pb}$ ,  $^{207}\text{Pb}$ - $^{235}\text{U}$  and  $^{206}\text{Pb}$ - $^{238}\text{U}$  ages. The different lines show the effect for different age measurement precisions, ranging from 2 to 0.01 %. Grey bands denote regions where the MSWD shift is not statistically significant (horizontal) or where  $^{207}\text{Pb}$ - $^{206}\text{Pb}$  ages are typically too imprecise to be relied upon (vertical). See *S8. Monte-Carlo simulations* for discussion.

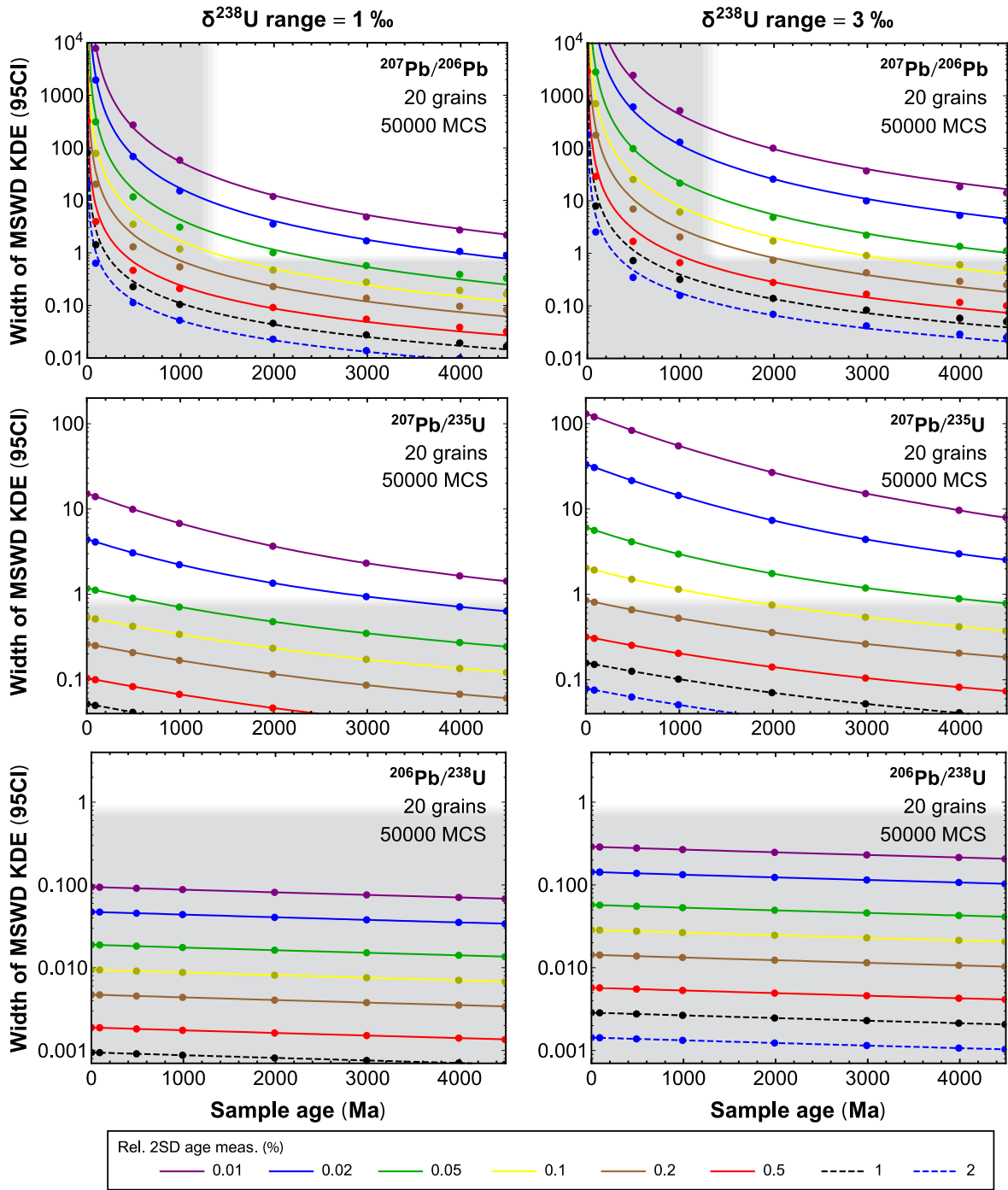


**Fig. S11.** Same as Fig. S10. but this time showing the width (95% confidence interval) of the U-corrected MSWD of the weighted mean ages of 20 grains. See *S8. Monte-Carlo simulations* for discussion.

**Table S1**

Amount of U (ng) released during the cleaning and digestion protocol.

Sample	Cleaning steps		Chemical abrasion	Residue digestion	Total	Percent of total U in each step			
	6.2 M HCl	5 M HNO <sub>3</sub>	28 M HF	28 M HF		HCl	HNO <sub>3</sub>	Chem. Abr.	Residue
<b>Bulk zircons</b>									
RSES72-1.3	0.56	0.03		33.18	33.77	1.66	0.10		98.24
RSES72-1.4	0.26	0.00		18.13	18.39	1.39	0.02		98.59
RSES72-1.7	0.10	b.d.l.		7.22	7.32	1.30	b.d.l.		98.70
RSES72-2.2	1.09	0.22		11.70	13.01	8.41	1.68		89.91
RSES72-2.3	0.44	0.00		33.79	34.23	1.30	0.00		98.71
RSES72-2.4	0.21	b.d.l.		12.91	13.13	1.63	b.d.l.		98.37
RSES72-2.6	0.56	0.18		21.82	22.56	2.48	0.80		96.72
RSES72-2.7	0.65	0.34		21.08	22.07	2.93	1.55		95.52
RSES72-3.7	0.51	0.15		24.63	25.29	2.01	0.61		97.39
RSES72-3.8	0.48	0.13		13.42	14.03	3.43	0.91		95.66
RSES72-5.6	0.78	0.19		14.80	15.77	4.98	1.19		93.83
RSES72-5.10	0.53	0.21		33.02	33.76	1.57	0.63		97.80
RSES72-6.1	0.18	0.11		19.60	19.89	0.92	0.53		98.55
RSES72-6.2	0.26	0.16		6.98	7.41	3.54	2.20		94.26
RSES72-6.4	0.08	0.06		2.52	2.67	3.14	2.39		94.47
RSES72-7.6	0.69	0.78		11.66	13.12	5.25	5.93		88.81
RSES72-9.3	0.46	0.09		7.06	7.61	6.05	1.14		92.81
RSES72-9.6	2.29	0.57		25.75	28.61	8.02	1.97		90.01
RSES72-9.8	2.98	2.03		19.88	24.89	11.96	8.17		79.86
RSES72-13.1	0.25	0.30		22.94	23.49	1.07	1.26		97.67
RSES72-13.4	0.08	0.01		2.10	2.19	3.72	0.48		95.80
RSES72-14.2	0.33	0.08		5.37	5.77	5.70	1.34		92.96
RSES72-14.3	0.14	0.09		3.24	3.47	4.16	2.51		93.34
RSES72-14.5	0.33	0.13		17.14	17.60	1.88	0.72		97.40
RSES72-18.2a	2.14	0.72		47.65	50.51	4.23	1.43		94.34
RSES72-18.2b	1.71	0.98		51.72	54.42	3.14	1.80		95.05
<b>Zircon standards</b>									
FC1 a				17.01	17.23	1.04	0.22		98.74
FC1 b	0.18	0.04		13.30	13.52	1.32	0.28		98.40
R33	0.07	0.11		6.87	7.05	1.02	1.57		97.41
Temora	0.17	0.06		7.10	7.33	2.36	0.83		96.82
<b>Zircon chemical abrasion (L) and residue (R)</b>									
RSES72-1.2	0.80	0.34	16.62	5.28	23.04	3.49	1.48	72.13	22.90
RSES72-3.6	0.48	0.12	24.80	1.89	27.29	1.75	0.43	90.88	6.94
RSES72-11.7	0.67	0.25	12.94	1.72	15.59	4.33	1.61	83.00	11.06
RSES72-18.3	0.33	0.05	7.76	25.08	33.22	1.00	0.14	23.36	75.50
RSES72-18.7	0.97	0.13	4.92	3.96	9.99	9.76	1.26	49.31	39.68
RSES72-18.10	0.72	0.12	6.24	3.07	10.15	7.04	1.21	61.46	30.28

**Table S2**

U and Zr content in the solutions used for U isotope analysis (post column chemistry).

Samples	U (ng)	Zr (ng)	Zr/U (wt/wt)	Zr/U (atomic)	U/Zr (atomic)
<b>Geostandards</b>					
BCR-2	276	1.8	0.006	0.017	59
CCH-1	293	1.9	0.006	0.017	60
DWA-1	307	1.6	0.005	0.014	74
<b>Zircons standards</b>					
FC-1 a	17.0	1.1	0.07	0.18	5.7
FC-1 b	13.3	1.8	0.13	0.35	2.8
R33	6.9	1.3	0.18	0.48	2.1
Temora	7.1	1.5	0.21	0.55	1.8
<b>Zircons (precleaned, not chemically abraded)</b>					
RSES72-2.6	21.8	2.7	0.12	0.33	3.1
RSES72-2.7	21.1	1.7	0.08	0.21	4.8
RSES72-3.7	24.6	1.6	0.07	0.17	5.8
RSES72-3.8	13.4	2.5	0.18	0.48	2.1
RSES72-5.6	14.8	2.7	0.19	0.48	2.1
RSES72-5.10	33.0	1.4	0.04	0.11	8.8
RSES72-6.1	19.6	1.7	0.09	0.23	4.3
RSES72-6.2	7.0	3.3	0.47	1.2	0.82
RSES72-6.4	2.5	2.5	0.98	2.6	0.39
RSES72-7.6	11.7	2.1	0.18	0.48	2.1
RSES72-9.3	7.1	1.6	0.23	0.61	1.6
RSES72-9.6	25.8	2.8	0.11	0.28	3.5
RSES72-9.8	19.9	1.2	0.06	0.16	6.4
RSES72-13.1	22.9	3.8	0.16	0.43	2.3
RSES72-13.4	2.1	3.2	1.5	4.0	0.25
RSES72-14.2	5.4	1.2	0.22	0.57	1.7
RSES72-14.3	3.2	1.4	0.43	1.1	0.89
RSES72-14.5	17.1	1.5	0.09	0.23	4.3
RSES72-18.2 a	47.7	2.1	0.04	0.11	8.8
RSES72-18.2 b	51.7	4.5	0.09	0.23	4.4
<b>Zircons chemical abrasion (L) and residues (R)</b>					
RSES72-1.2 L	14.6	3.9	0.27	0.69	1.4
RSES72-1.2 R	5.3	1.4	0.27	0.71	1.4
RSES72-3.6 L	21.2	2.1	0.10	0.26	3.8
RSES72-3.6 R	1.9	3.7	2.0	5.2	0.19
RSES72-11.7 L	11.2	2.6	0.23	0.61	1.7
RSES72-11.7 R	1.7	4.2	2.4	6.4	0.16
RSES72-18.3 L	6.9	3.2	0.46	1.2	0.83
RSES72-18.3 R	25.1	1.9	0.08	0.20	5.0
RSES72-18.7 L	4.5	3.2	0.71	1.8	0.54
RSES72-18.7 R	4.0	1.4	0.34	0.89	1.1
RSES72-18.10 L	5.8	3.1	0.54	1.4	0.72
RSES72-18.10 R	3.1	2.1	0.67	1.8	0.57
<b>Blanks</b>					
Blank bulk	0.26	1.9	7.3	19	0.052
Blank chem. abr.	0.18	2.0	11.3	30	0.034
Blank residue	0.19	1.8	9.3	24	0.041

**Table S3**

U isotopic compositions and concentrations of selected geostandards.

Sample	Setup	Resin #	Bk (ng)	<sup>232</sup> Th (mV)	<sup>238</sup> U (V)	Zr/U (atom)	ng U	n	Total cycles	Double-spike data reduction				Sample-standard bracketing		
										δ <sup>238</sup> U (‰)	δ( <sup>234</sup> U) (‰)	Conc. (ug/g)	Usp/Uamp	δ <sup>238</sup> U (‰)	δ( <sup>234</sup> U) (‰)	
<b>Basalt</b>																
BCR-2 a	MIT	2	0.005	0.3	42	n.m	250	1	60	-0.27 ± 0.24	0.5 ± 3.3	1.733 ± 0.004	5.0%	-0.24 ± 0.65	1.6 ± 3.0	
BCR-2 a	MIT	2	0.005	0.3	30			5	300	-0.22 ± 0.07	-0.1 ± 3.4	1.732 ± 0.004	5.0%	0.02 ± 0.33	-3.2 ± 3.1	
BCR-2 a	MIT	2	0.005	0.1	23			1	60	-0.21 ± 0.18	3.1 ± 9.0	1.731 ± 0.004	5.0%	-0.26 ± 0.82	2.2 ± 11.7	
BCR-2 a	MIT	2	0.005	0.3	20			2	119	-0.27 ± 0.11	-2.9 ± 9.1	1.731 ± 0.004	5.0%	-0.28 ± 0.50	-5.5 ± 8.7	
<i>Weighted average</i>									<b>9</b>		<b>-0.23 ± 0.06</b>	<b>0.2 ± 2.2</b>	<b>1.732 ± 0.002</b>	<b>5.0%</b>	<b>-0.11 ± 0.24</b>	<b>-0.9 ± 2.1</b>
BCR-2 b	MIT	2	0.005	0.7	41	n.m	248	2	120	-0.16 ± 0.17	2.7 ± 2.4	1.731 ± 0.004	5.3%	-0.09 ± 0.46	3.4 ± 2.1	
BCR-2 b	MIT	2	0.005	0.7	42			2	120	-0.27 ± 0.10	4.2 ± 6.2	1.730 ± 0.004	5.3%	-0.16 ± 0.53	4.9 ± 6.5	
BCR-2 b	MIT	2	0.005	0.3	13			2	120	-0.28 ± 0.13	4.0 ± 21.1	1.730 ± 0.004	5.3%	-0.01 ± 0.60	0.6 ± 20.6	
BCR-2 b	MIT	2	0.005	0.3	13			8	479	-0.28 ± 0.06	3.7 ± 10.5	1.730 ± 0.004	5.3%	-0.06 ± 0.30	-2.0 ± 10.3	
BCR-2 b	MIT	2	0.005	0.2	3.8			8	480	-0.33 ± 0.24	7.0 ± 39.0	1.730 ± 0.004	5.3%	-0.32 ± 0.28	3.6 ± 38.0	
<i>Weighted average</i>									<b>22</b>		<b>-0.27 ± 0.05</b>	<b>2.9 ± 2.1</b>	<b>1.730 ± 0.002</b>	<b>5.3%</b>	<b>-0.16 ± 0.17</b>	<b>3.3 ± 2.0</b>
BCR-2 c	O.L.	2	0.017	2.9	20	n.m	251	1	55	-0.27 ± 0.34	-0.3 ± 1.6	1.728 ± 0.006	2.8%	-0.42 ± 0.38	-0.6 ± 2.1	
BCR-2 c	O.L.	2	0.017	1.6	14			2	110	-0.25 ± 0.10	0.1 ± 0.7	1.729 ± 0.006	2.8%	-0.21 ± 0.18	-0.5 ± 0.7	
BCR-2 c	O.L.	2	0.017	1.8	16			1	50	-0.24 ± 0.20	0.3 ± 0.6	1.728 ± 0.006	2.8%	-0.29 ± 0.16	-0.1 ± 0.5	
BCR-2 c	O.L.	2	0.017	2.1	17			2	100	-0.30 ± 0.09	0.0 ± 0.5	1.728 ± 0.006	2.8%	-0.27 ± 0.22	-0.5 ± 0.5	
BCR-2 c	O.L.	2	0.017	2.3	17			2	100	-0.27 ± 0.15	-0.2 ± 0.8	1.728 ± 0.006	2.8%	-0.31 ± 0.14	-0.7 ± 0.8	
BCR-2 c	O.L.	2	0.017	1.2	13			3	150	-0.21 ± 0.08	-0.3 ± 0.4	1.728 ± 0.006	2.8%	-0.06 ± 0.24	-1.0 ± 0.5	
BCR-2 c	O.L.	2	0.017	1.8	19			2	100	-0.35 ± 0.11	-0.1 ± 0.6	1.728 ± 0.006	2.8%	-0.30 ± 0.12	-0.7 ± 0.6	
<i>Weighted average</i>									<b>13</b>		<b>-0.27 ± 0.04</b>	<b>0.0 ± 0.2</b>	<b>1.728 ± 0.002</b>	<b>2.8%</b>	<b>-0.27 ± 0.06</b>	<b>-0.6 ± 0.2</b>
BCR-2 d	O.L.	2	0.010	0.02	11	0.017	254	4	200	-0.25 ± 0.08	0.9 ± 0.3	1.727 ± 0.006	2.9%	-0.18 ± 0.26	0.8 ± 0.4	
BCR-2 d	O.L.	2	0.010	0.03	17			2	100	-0.30 ± 0.09	0.9 ± 0.9	1.726 ± 0.006	2.9%	-0.16 ± 1.14	0.7 ± 1.5	
BCR-2 d	O.L.	2	0.010	0.04	17			3	150	-0.25 ± 0.13	0.7 ± 0.5	1.727 ± 0.006	2.9%	-0.16 ± 0.14	0.5 ± 0.5	
BCR-2 d	O.L.	2	0.010	0.04	18			2	100	-0.31 ± 0.15	1.1 ± 0.9	1.726 ± 0.006	2.9%	-0.24 ± 0.41	1.0 ± 1.2	
BCR-2 d	O.L.	2	0.010	0.04	17			2	100	-0.22 ± 0.09	0.7 ± 0.5	1.727 ± 0.006	2.9%	-0.18 ± 0.11	0.6 ± 0.5	
<i>Weighted average</i>									<b>13</b>		<b>-0.26 ± 0.04</b>	<b>0.8 ± 0.2</b>	<b>1.727 ± 0.003</b>	<b>2.9%</b>	<b>-0.17 ± 0.08</b>	<b>0.7 ± 0.3</b>
<b>Crinoïdic limestone</b>																
CCH-1	O.L.	2	0.017	0.02	11	0.017	253	1	55	-0.08 ± 0.14	-1.6 ± 1.0	3.82 ± 0.02	2.8%	-0.17 ± 0.25	-2.0 ± 1.0	
CCH-1	O.L.	2	0.017	0.03	12			1	50	-0.04 ± 0.20	-2.3 ± 0.6	3.82 ± 0.02	2.8%	-0.18 ± 0.16	-2.5 ± 0.5	
CCH-1	O.L.	2	0.017	0.02	13			2	100	-0.08 ± 0.09	-1.6 ± 0.5	3.82 ± 0.02	2.8%	-0.07 ± 0.22	-2.1 ± 0.5	
CCH-1	O.L.	2	0.017	0.04	14			1	50	0.06 ± 0.22	-2.2 ± 1.2	3.82 ± 0.02	2.8%	0.11 ± 0.20	-2.7 ± 1.1	
CCH-1	O.L.	2	0.017	0.03	15			2	100	-0.07 ± 0.11	-2.4 ± 0.6	3.82 ± 0.02	2.8%	-0.05 ± 0.12	-2.9 ± 0.6	
<i>Weighted average</i>									<b>7</b>		<b>-0.07 ± 0.06</b>	<b>-2.0 ± 0.3</b>	<b>3.82 ± 0.01</b>	<b>2.8%</b>	<b>-0.07 ± 0.08</b>	<b>-2.5 ± 0.3</b>
<b>Dolomite</b>																
DWA-1	O.L.	2	0.017	0.01	11	0.014	268	1	55	-0.30 ± 0.14	-7.2 ± 1.0	1.479 ± 0.005	2.7%	-0.15 ± 0.25	-7.8 ± 1.0	
DWA-1	O.L.	2	0.017	0.02	12			1	50	-0.13 ± 0.20	-6.6 ± 0.6	1.479 ± 0.005	2.7%	-0.17 ± 0.16	-6.9 ± 0.5	
DWA-1	O.L.	2	0.017	0.02	13			1	50	-0.14 ± 0.13	-6.7 ± 0.7	1.479 ± 0.005	2.7%	-0.15 ± 0.30	-7.1 ± 0.7	
DWA-1	O.L.	2	0.017	0.03	20			4	200	-0.20 ± 0.08	-7.3 ± 0.4	1.479 ± 0.005	2.7%	-0.15 ± 0.08	-7.7 ± 0.4	
<i>Weighted average</i>									<b>7</b>		<b>-0.20 ± 0.06</b>	<b>-7.0 ± 0.3</b>	<b>1.479 ± 0.002</b>	<b>2.7%</b>	<b>-0.15 ± 0.07</b>	<b>-7.4 ± 0.3</b>

n.m. stands for "not measured".

MIT: Measurement made at the McGee Lab (MIT) on a Nu-Plasma II.Cup configuration for <sup>232</sup>Th/<sup>233</sup>U/<sup>234</sup>U/<sup>235</sup>U/<sup>236</sup>U/<sup>238</sup>U as L4/L3/L2/L1/Ax/H2

O.L.: Measurement made at the Origins Lab (U. of Chicago) on a Neptune MC-ICPMS. Cup configuration for <sup>232</sup>Th/<sup>233</sup>U/<sup>234</sup>U/<sup>235</sup>U/<sup>236</sup>U/<sup>238</sup>U as L2/L1/SEM/H1/H2/H3

Tailing from <sup>238</sup>U on <sup>236</sup>U, <sup>235</sup>U and <sup>234</sup>U was taken as, respectively, 0.6 ppm, 0.25 ppm and 0.1 ppm. Hydride formation was corrected using the value <sup>238</sup>U/<sup>238</sup>U = 7.3e-7. Activity ratio [<sup>234</sup>U/<sup>238</sup>U] of the sample relative to secular equilibrium (in ‰). δ(<sup>234</sup>U) = { (234U/238U)<sub>smp</sub> / (234U/238U)<sub>eq</sub> - 1 } \* 1000 where (234U/238U)<sub>eq</sub> is the atomic ratio at secular equilibrium and is equal to λ<sup>238</sup>U/λ<sup>234</sup>U = 5.4969e-5 (Cheng et al., 2013).

Table S4

U isotopic compositions of Archean and Hadean zircons.

Sample	Setup	Resin #	Bk (ng)	<sup>232</sup> Th (mV)	<sup>238</sup> U (V)	Zr/U (atomic)	ng U	n	Total cycles	Double-spike data reduction			Sample-standard bracketing	
										$\delta^{238}\text{U}$ (‰)	$\delta^{234}\text{U}$ (‰)	Usp/Usm	$\delta^{238}\text{U}$ (‰)	$\delta^{234}\text{U}$ (‰)
<b>Bulk Zircons</b>														
RSES72-1.3	MIT	2	0.011	2.2	19	n.m	33.2	2	120	-0.28 ± 0.11	-214.6 ± 9.1	3.1%	-0.49 ± 0.50	-210.3 ± 8.7
RSES72-1.4	MIT	2	0.011	0.4	18	n.m	18.1	1	60	-0.24 ± 0.16	-30.3 ± 12.9	3.1%	-0.36 ± 0.71	-30.5 ± 12.4
RSES72-1.7	MIT	2	0.011	2.4	11	n.m	7.2	1	36	-0.25 ± 0.18	-85.8 ± 29.8	3.5%	-0.37 ± 0.84	-85.0 ± 29.1
RSES72-2.2	MIT	2	0.011	0.6	10	n.m	11.7	2	115	-0.52 ± 0.17	-299.2 ± 28.8	3.2%	-0.75 ± 0.58	-292.2 ± 28.1
RSES72-2.3	MIT	2	0.011	2.2	19	n.m	33.8	2	120	-0.22 ± 0.11	-280.8 ± 9.1	3.3%	-0.27 ± 0.50	-275.3 ± 8.7
RSES72-2.4	MIT	2	0.011	1.7	11	n.m	12.9	2	115	-0.29 ± 0.17	-280.5 ± 24.9	3.3%	-0.44 ± 0.31	-274.3 ± 24.3
RSES72-2.6	O.L.	2	0.017	1.5	15	0.325	21.8	5	255	-0.29 ± 0.07	-285.3 ± 0.3	2.8%	-0.16 ± 0.12	-282.2 ± 0.3
RSES72-2.7	O.L.	2	0.017	3.1	15	0.210	21.1	5	255	-0.18 ± 0.07	-251.6 ± 0.3	2.7%	-0.18 ± 0.12	-248.9 ± 0.3
RSES72-3.7	O.L.	2	0.017	0.37	16	0.173	24.6	6	300	-0.20 ± 0.06	-339.8 ± 0.3	2.8%	-0.11 ± 0.13	-336.2 ± 0.3
RSES72-3.8	O.L.	2	0.017	0.16	17	0.481	13.4	4	171	-0.24 ± 0.07	-194.1 ± 0.4	2.7%	-0.18 ± 0.18	-192.2 ± 0.4
RSES72-5.6	O.L.	2	0.010	0.52	17	0.483	14.8	4	173	-0.26 ± 0.08	-290.0 ± 0.6	3.8%	-0.25 ± 0.20	-287.2 ± 0.6
RSES72-5.10	O.L.	2	0.017	0.14	20	0.114	33.0	8	391	-0.18 ± 0.05	-179.9 ± 0.3	2.8%	-0.13 ± 0.10	-178.2 ± 0.3
RSES72-6.1	O.L.	2	0.017	0.37	16	0.230	19.6	5	239	-0.12 ± 0.06	-125.7 ± 0.3	2.8%	-0.07 ± 0.12	-124.7 ± 0.3
RSES72-6.2	O.L.	2	0.017	0.41	15	1.218	7.0	2	88	-0.39 ± 0.09	-182.4 ± 0.5	2.9%	-0.32 ± 0.22	-180.8 ± 0.5
RSES72-6.4	O.L.	2	0.017	1.3	11	2.568	2.5	1	35	-0.25 ± 0.22	-223.7 ± 1.2	3.1%	-0.06 ± 0.21	-221.6 ± 1.1
RSES72-7.6	O.L.	2	0.010	2.6	16	0.478	11.7	3	150	-0.26 ± 0.10	-198.0 ± 0.5	3.9%	-0.23 ± 0.17	-194.7 ± 0.5
RSES72-9.3	O.L.	2	0.010	0.35	18	0.609	7.1	2	92	-0.31 ± 0.13	-178.7 ± 0.5	3.7%	-0.17 ± 0.22	-177.2 ± 0.6
RSES72-9.6	O.L.	2	0.010	0.16	16	0.282	25.8	7	325	-0.30 ± 0.07	-270.1 ± 0.3	3.9%	-0.22 ± 0.13	-267.3 ± 0.3
RSES72-9.8	O.L.	2	0.010	0.58	16	0.156	19.9	5	243	-0.40 ± 0.07	-299.7 ± 0.3	3.8%	-0.30 ± 0.18	-296.5 ± 0.4
RSES72-13.1	O.L.	2	0.010	0.28	16	0.429	22.9	6	290	-0.33 ± 0.08	-212.8 ± 0.4	3.8%	-0.27 ± 0.15	-210.5 ± 0.5
RSES72-13.4	O.L.	2	0.010	2.7	14	3.987	2.1	1	21	-0.32 ± 0.25	-37.6 ± 1.5	3.9%	-0.49 ± 1.74	-37.3 ± 2.3
RSES72-14.2	O.L.	2	0.017	0.61	16	0.574	5.4	2	62	-0.19 ± 0.11	-175.6 ± 0.6	3.0%	-0.15 ± 0.17	-173.8 ± 0.6
RSES72-14.3	O.L.	2	0.017	1.4	15	1.126	3.2	1	42	-0.26 ± 0.14	-220.7 ± 0.8	2.9%	-0.10 ± 0.33	-218.7 ± 0.7
RSES72-14.5	O.L.	2	0.017	0.20	15	0.234	17.1	4	200	-0.29 ± 0.09	-277.3 ± 0.5	2.7%	-0.21 ± 0.11	-274.4 ± 0.5
RSES72-18.2a	O.L.	2	0.010	0.89	16	0.114	47.7	12	600	-0.30 ± 0.05	-123.9 ± 0.2	3.8%	-0.22 ± 0.06	-122.8 ± 0.2
RSES72-18.2b	O.L.	2	0.010	0.20	15	0.228	51.7	13	650	-0.30 ± 0.04	-86.3 ± 0.2	3.8%	-0.25 ± 0.06	-85.7 ± 0.2
<b>Weighted average</b>										<b>-0.30 ± 0.03</b>			<b>-0.24 ± 0.04</b>	
<b>Zircon standards</b>														
FC-1 a	O.L.	2	0.017	0.27	16	0.176	17.0	5	213	-0.15 ± 0.09	-0.4 ± 0.5	2.7%	-0.04 ± 0.09	-2.9 ± 0.6
FC-1 b	O.L.	2	0.017	0.55	15	0.352	13.3	4	166	-0.03 ± 0.09	-0.5 ± 0.5	2.9%	0.06 ± 0.09	-1.1 ± 0.5
<b>Weighted average</b>										<b>-0.10 ± 0.06</b>			<b>0.01 ± 0.06</b>	
R33	O.L.	2	0.017	2.3	17	0.478	6.9	2	82	-0.14 ± 0.11	2.1 ± 0.6	2.8%	-0.10 ± 0.17	1.5 ± 0.6
Temora	O.L.	2	0.017	0.51	15	0.548	7.1	2	87	-0.07 ± 0.15	-0.3 ± 0.8	2.8%	-0.06 ± 0.14	-0.8 ± 0.8
<b>Zircon chemical abrasion (L) and residue (R)</b>														
RSES72-1.2 L	O.L.	2	0.010	1.8	16	0.692	14.6	4	183	-0.36 ± 0.08	-267.7 ± 0.3	4.0%	-0.60 ± 0.24	-264.6 ± 0.5
RSES72-1.2 R	O.L.	2	0.010	0.54	17	0.712	5.3	2	67	-0.12 ± 0.13	1.2 ± 0.6	3.9%	-0.29 ± 0.32	0.8 ± 0.7
RSES72-3.6 L	O.L.	2	0.010	0.17	16	0.264	21.2	6	268	-0.40 ± 0.07	-264.6 ± 0.3	3.8%	-0.44 ± 0.16	-261.7 ± 0.4
RSES72-3.6 R	O.L.	2	0.010	3.4	11	5.150	1.9	1	20	-0.60 ± 0.22	185.0 ± 1.4	4.0%	-0.43 ± 0.26	181.7 ± 1.4
RSES72-11.7 L	O.L.	2	0.010	0.21	17	0.606	11.2	3	148	-0.40 ± 0.09	-263.5 ± 0.6	3.9%	-0.27 ± 0.23	-260.7 ± 0.7
RSES72-11.7 R	O.L.	2	0.010	2.3	12	6.383	1.7	1	18	-0.37 ± 0.25	20.3 ± 1.5	3.9%	0.00 ± 1.74	19.2 ± 2.3
RSES72-18.3 L	O.L.	2	0.010	0.48	16	1.207	6.9	2	84	-0.17 ± 0.12	-147.7 ± 0.8	3.8%	-0.19 ± 0.24	-146.7 ± 0.8
RSES72-18.3 R	O.L.	2	0.010	0.19	16	0.202	25.1	7	313	-0.10 ± 0.08	-1.6 ± 0.4	3.8%	0.01 ± 0.14	-2.1 ± 0.5
RSES72-18.7 L	O.L.	2	0.010	1.3	15	1.845	4.5	1	50	-0.19 ± 0.13	-299.7 ± 1.3	3.9%	0.40 ± 1.61	-297.8 ± 2.1
RSES72-18.7 R	O.L.	2	0.010	9.3	14	0.892	4.0	1	50	-0.11 ± 0.13	17.1 ± 1.3	3.9%	-0.30 ± 1.61	17.0 ± 2.1
RSES72-18.10 L	O.L.	2	0.010	0.91	14	1.398	5.8	2	70	-0.28 ± 0.12	-132.0 ± 1.0	3.9%	-0.23 ± 0.40	-131.7 ± 1.3
RSES72-18.10 R	O.L.	2	0.010	1.1	13	1.756	3.1	1	37	-0.23 ± 0.18	23.4 ± 1.5	3.8%	-1.27 ± 1.67	24.5 ± 2.1

n.m. stands for "not measured".

MIT: Measurement made at the McGee Lab (MIT) on a Nu-Plasma II.Cup configuration for <sup>232</sup>Th/<sup>233</sup>U/<sup>234</sup>U/<sup>235</sup>U/<sup>236</sup>U/<sup>238</sup>U as L4/L3/L2/L1/Ax/H2O.L.: Measurement made at the Origins Lab (U. of Chicago) on a Neptune MC-ICPMS. Cup configuration for <sup>232</sup>Th/<sup>233</sup>U/<sup>234</sup>U/<sup>235</sup>U/<sup>236</sup>U/<sup>238</sup>U as L2/L1/SEM/H1/H2/H3Tailing from <sup>238</sup>U on <sup>236</sup>U, <sup>235</sup>U and <sup>234</sup>U was taken as, respectively, 0.6 ppm, 0.25 ppm and 0.1 ppm. Hydride formation was corrected using the value <sup>238</sup>UH/<sup>238</sup>U = 7.3e-7.Activity ratio [<sup>234</sup>U/<sup>238</sup>U] of the sample relative to secular equilibrium (in ‰),  $\delta^{234}\text{U} = \{ (234\text{U}/238\text{U})_{\text{sm}} / (234\text{U}/238\text{U})_{\text{eq}} - 1 \} * 1000$  where (234U/238U)<sub>eq</sub> is the atomic ratio at secular equilibrium and is equal to  $\lambda^{238}\text{U} / \lambda^{234}\text{U} = 5.4969\text{e-}5$  (Cheng et al., 2013).For the spiking levels used in this study (between 2.7 and 4.0 %), the proportion of <sup>234</sup>U from the spike in the spike + sample mixture analyzed ranged from 8.5 to 12.1 %.

**Table S5**

Comparison of U isotope data for bulk zircons (i.e., not chemically abraded) with published literature.

Sample	This Work			Hiess et al. (2012)			Livermore et al. (2018)**		
	$\delta^{238}\text{U}$ (‰)	$^{238}\text{U}/^{235}\text{U}$	$\delta(^{234}\text{U})$ (‰)	$\delta^{238}\text{U}$ (‰)	$^{238}\text{U}/^{235}\text{U}$	$\delta(^{234}\text{U})$ (‰)	$\delta^{238}\text{U}$ (‰)	$^{238}\text{U}/^{235}\text{U}$	$\delta(^{234}\text{U})$ (‰)
FC-1	-0.10 ±0.06	137.824 ±0.009	-0.5 ±0.3	-0.05 ±0.06	137.830 ±0.008	-2.0 ±5.0			
R33	-0.14 ±0.11	137.817 ±0.016	2.1 ±0.6	-0.15 ±0.06	137.816 ±0.008	-3.6 ±4.8	-0.13 ±0.02	137.819 ±0.003	
Temora*	-0.07 ±0.15	137.828 ±0.021	-0.3 ±0.8	-0.14 ±0.04	137.818 ±0.006	-2.8 ±3.4	-0.02 ±0.02	137.834 ±0.003	

\* As no bulk zircon data was reported in Hiess et al. (2012), the residue value is used here for comparison.

\*\* As no bulk zircon data was reported in Livermore et al. (2018), the residue value is used here for comparison.

d<sup>238</sup>U values are relative to CRM-112a.

238U/235U values are calculated assuming a 238U/235U ratio of 137.837 in CRM-112a (Richter et al., 2010)

Activity ratio [234U/238U] of the sample relative to secular equilibrium (in ‰).  $d(^{234}\text{U}) = \left\{ \frac{(^{234}\text{U}/^{238}\text{U})_{\text{smp}}}{(^{234}\text{U}/^{238}\text{U})_{\text{eq}}} - 1 \right\} * 1000$  where  $(^{234}\text{U}/^{238}\text{U})_{\text{eq}}$  is the atomic ratio at secular equilibrium and is equal to  $\lambda^{238}\text{U}/\lambda^{234}\text{U} = 5.4969\text{e-}5$  (Cheng et al., 2013).

## References

- Albarede, F., Telouk, P., Blichert-Toft, J., Boyet, M., Agranier, A., Nelson, B., 2004. Precise and accurate isotopic measurements using multiple-collector ICPMS. *Geochim Cosmochim Acta* 68, 2725-2744.
- Amelin, Y., 2006. The prospect of high-precision Pb isotopic dating of meteorites. *Meteorit Planet Sci* 41, 7-17.
- Barboni, M., Boehnke, P., Keller, B., Kohl, I.E., Schoene, B., Young, E.D., McKeegan, K.D., 2017. Early formation of the Moon 4.51 billion years ago. *Sci Adv* 3.
- Black, L.P., Kamo, S.L., Allen, C.M., Davis, D.W., Aleinikoff, J.N., Valley, J.W., Mundil, R., Campbell, I.H., Korsch, R.J., Williams, I.S., Foudoulis, C., 2004. Improved (206)Pb/(238)U microprobe geochronology by the monitoring of a trace-element-related matrix effect; SHRIMP, ID-TIMS, ELA-ICP-MS and oxygen isotope documentation for a series of zircon standards. *Chemical Geology* 205, 115-140.
- Burgess, S.D., Bowring, S., Shen, S.Z., 2014. High-precision timeline for Earth's most severe extinction. *Proceedings of the National Academy of Sciences of the United States of America* 111, 3316-3321.
- Cheng, H., Edwards, R.L., Shen, C.C., Polyak, V.J., Asmerom, Y., Woodhead, J., Hellstrom, J., Wang, Y.J., Kong, X.G., Spotl, C., Wang, X.F., Alexander, E.C., 2013. Improvements in Th-230 dating, Th-230 and U-234 half-life values, and U-Th isotopic measurements by multi-collector inductively coupled plasma mass spectrometry. *Earth Planet Sc Lett* 371, 82-91.
- Dauphas, N., Chen, J.H., Zhang, J.J., Papanastassiou, D.A., Davis, A.M., Travaglio, C., 2014. Calcium-48 isotopic anomalies in bulk chondrites and achondrites: Evidence for a uniform isotopic reservoir in the inner protoplanetary disk. *Earth Planet Sc Lett* 407, 96-108.
- Fairchild, L.M., Swanson-Hysell, N.L., Ramezani, J., Sprain, C.J., Bowring, S.A., 2017. The end of Midcontinent Rift magmatism and the paleogeography of Laurentia. *Lithosphere-US* 9, 117-133.
- Hiess, J., Condon, D.J., McLean, N., Noble, S.R., 2012. U-238/U-235 Systematics in Terrestrial Uranium-Bearing Minerals. *Science* 335, 1610-1614.
- Holden, P., Lanc, P., Ireland, T.R., Harrison, T.M., Foster, J.J., Bruce, Z., 2009. Mass-spectrometric mining of Hadean zircons by automated SHRIMP multi-collector and single-collector U/Pb zircon age dating: The first 100,000 grains. *International Journal of Mass Spectrometry* 286, 53-63.
- Jaffey, A.H., Flynn, K.F., Glendenin, L.E., Bentley, W.C., Essling, A.M., 1971. Precision Measurement of Half-Lives and Specific Activities of U-235 and U-238. *Phys Rev C* 4, 1889-1906.
- Livermore, B.D., Connelly, J.N., Moynier, F., Bizzarro, M., 2018. Evaluating the robustness of a consensus U-238/U-235 value for U-Pb geochronology. *Geochim Cosmochim Acta* 237, 171-183.
- Mahon, K.I., 1996. The New "York" regression: Application of an improved statistical method to geochemistry. *Int Geol Rev* 38, 293-303.
- Mattinson, J.M., 2010. Analysis of the relative decay constants of U-235 and U-238 by multi-step CA-TIMS measurements of closed-system natural zircon samples. *Chemical Geology* 275, 186-198.

Paces, J.B., Miller, J.D., 1993. Precise U-Pb Ages of Duluth Complex and Related Mafic Intrusions, Northeastern Minnesota - Geochronological Insights to Physical, Petrogenetic, Paleomagnetic, and Tectonomagmatic Processes Associated with the 1.1 Ga Midcontinent Rift System. *J Geophys Res-Sol Ea* 98, 13997-14013.

Richter, S., Eykens, R., Kuhn, H., Aregbe, Y., Verbruggen, A., Weyer, S., 2010. New average values for the  $n(\text{U-238})/n(\text{U-235})$  isotope ratios of natural uranium standards. *International Journal of Mass Spectrometry* 295, 94-97.

Schmitz, M.D., Schoene, B., 2007. Derivation of isotope ratios, errors, and error correlations for U-Pb geochronology using Pb-205-U-235-(U-233)-spiked isotope dilution thermal ionization mass spectrometric data. *Geochem Geophys Geosy* 8.

Steiger, R.H., Jager, E., 1977. Subcommittee on Geochronology - Convention on Use of Decay Constants in Geochronology and Cosmochronology. *Earth Planet Sc Lett* 36, 359-362.

Tissot, F.L.H., Dauphas, N., 2015. Uranium isotopic compositions of the crust and ocean: Age corrections, U budget and global extent of modern anoxia. *Geochim Cosmochim Acta* 167, 113-143.

Verbruggen, A., Alonso, A., Eykens, R., Kehoe, F., Kuhn, H., Richter, S., Aregbe, Y., 2008. Preparation and certification of IRMM-3636, IRMM-3636a and IRMM-3636b. JRC Scientific and Technical Reports.